ENHANCING THE RESOLUTION OF SEA ICE IN LONG-TERM GLOBAL OCEAN GENERAL CIRCULATION MODEL (GCM) INTEGRATIONS

A Dissertation

by

JOONG TAE KIM

Submitted to the Office of Graduate Studies of
Texas A&M University
in partial fulfillment of the requirements for the degree of

DOCTOR OF PHILOSOPHY

May 2007

Major Subject: Oceanography

ENHANCING THE RESOLUTION OF SEA ICE IN LONG-TERM GLOBAL OCEAN GENERAL CIRCULATION MODEL (GCM) INTEGRATIONS

A Dissertation

by

JOONG TAE KIM

Submitted to the Office of Graduate Studies of
Texas A&M University
in partial fulfillment of the requirements for the degree of

DOCTOR OF PHILOSOPHY

Approved by:

Chair of Committee,	Achim Stössel
Committee Members,	Ping Chang
	Benjamin Giese
	Thomas Wilheit
Head of Department,	Robert Stickney

May 2007

Major Subject: Oceanography

ABSTRACT

Enhancing the Resolution of Sea Ice in Long-Term Global Ocean General Circulation Model (GCM) Integrations. (May 2007)

Joong Tae Kim, B.S., Hanyang University;
M.S., Ohio University
Chair of Advisory Committee: Dr. Achim Stössel

Open water in sea ice, such as leads and polynyas, plays a crucial role in determining the formation of deep- and bottom-water, as well as their long-term global properties and circulation. Ocean general circulation models (GCMs) designed for studies of the long-term thermohaline circulation have typically coarse resolution, making it inevitable to parameterize subgrid-scale features such as leads and convective plumes. In this study, a hierarchy of higher-resolution sea-ice models is developed to reduce uncertainties due to coarse resolution, while keeping the ocean component at coarse resolution to maintain the efficiency of the GCM to study the long-term deep-ocean properties and circulation. The higher-resolved sea-ice component is

restricted to the Southern Ocean. Compared with the coarse sea-ice model, the intermediate, higher-resolution version yields more detailed coastal polynyas, a realistically sharp ice edge, and an overall enhanced lead fraction. The latter gives enhanced rates of Antarctic Bottom Water formation through enhanced near-boundary convection. Sensitivity experiments revealed coastal katabatic winds accounted for in the higher resolution version, are the main reason for producing such an effect. For a more realistic coastline, satellite passive-microwave data for fine-grid land/ice-shelf - sea-ice/ocean boundary were used.

With a further enhancement of the resolution of the Southern Ocean's sea-ice component, a grid spacing of 22 km is reached. This is about the size of the pixel resolution of satellite-passive microwave data from which ice concentration is retrieved. This product is used in this study to validate the sea-ice component of the global ocean GCM. The overall performance of the high-resolution sea-ice component is encouraging, particularly the representation of the crucial coastal

polynyas. Enhancing the resolution of the convection parameterization reduces spurious coarse-grid polynyas. Constraining the upper-ocean temperature and modifying the plume velocity removes unrealistic small-scale convection within the ice pack. The observed high-frequency variability along the ice edge is to some extent captured by exposing the ice pack to upper-ocean currents that mimic tidal variability. While these measures improve several characteristics of the Southern Ocean sea-ice pack, they deteriorate the global deep-ocean properties and circulation, calling for further refinements and tuning to arrive at presently observed conditions.

DEDICATION

This dissertation is dedicated to my father the late Jong Dae Kim and to my mother Jung Soon Park. Without their love and support, I cannot do anything. This is also dedicated to my wife Yu Jung Jang, son Dohun and daughter Jenna. I love all of them.

"gate gate paragate parasamgate bhodi svaha"

ACKNOWLEDGMENTS

I am grateful to my committee chair Dr. Achim Stössel. His direct and indirect support, guidance and encouragement enabled me to finish my study. Not only his insight of ocean climate modeling but also his precise view of life helped to enlighten my life.

I thank my committee members, Dr. Giese, Dr. Wilheit, and Dr. Chang, for their advice regarding this study and life experiences. I thank my colleagues who helped me finish this study.

NASA's research grant NAG5-10641 and NSF's research grant ATM-0333341 support my study.

TABLE OF CONTENTS

Page

CHAPTER

LIST OF TABLES

LIST OF FIGURES

FIGURE Page

CHAPTER I

INTRODUCTION

High-latitude surface conditions play a crucial role in determining the long-term deep-ocean properties and circulation of the world's ocean (e.g., Maier-Reimer, 1993; Broecker, 1997; Duffy et al., 1999; Goosse et al., 2001; Orsi et al., 2001; Stössel et al., 2002). In general, heavier water flows under lighter water due to gravity. Cold air at high latitudes contacts the sea-surface directly so that water is cooled to the freezing point, and sea ice is formed. This has several characteristics related to the sea water interactions by dynamics and thermodynamics. Sea ice has high albedo which reflects about 30 to 40 % of incoming short wave solar energy and if sea ice is covered by snow even more up to 80 to 90 % of solar energy is reflected. Sea ice prevents direct contact between cold air and the relative warm sea water. While the open ocean looses a lot of heat

---

This dissertation follows the style and format of Ocean Modelling.

energy to the air, an ice covered ocean looses much less heat energy by conduction because the thermal conductivity of ice is much lower. Furthermore, ice can hardly hold salt, therefore when new sea ice forms, brine is released which makes the surface water dense, resulting in buoyancy loss and possibly sinking. In winter, open ocean in ice pack is the major place to produce dense water by heat energy loss and brine release. The rejected brine increases the density of the surface water. Both cooled water and brine increase the density of the sea surface. The cold or salty heavy water at the sea surface starts to sink to a depth where its density is equilibrated to the surrounding water. This sinking cold or salty heavy water flows from the polar regions to fill the deep ocean basins, rises to the surface in the low latitude, then, flows poleward to replace the water which has sunk to the bottom. This circulation pattern is called thermohaline circulation (THC). THC follows a conveyor-belt circulation pattern (Stommel, 1962; Killworth, 1983; Broecker, 1991). The two regions of deep-water formation are the northern North Atlantic Ocean and the Southern

Ocean continental margin. For the northern North Atlantic Ocean, the major source of the deep water is the overflow from the Norwegian Sea over the sills between Greenland and Scotland. At the Southern Ocean continental margin, the main source is the Weddell Sea where sinking results from density increased by the brine rejection during sea-ice formation. Other sources around Antarctica are the Ross Sea in the South Pacific Ocean and the Adélie Coast. Coastal polynyas and open ocean polynyas are the important locations of dense water formation. The formation of deep water is intermittent even during the cooling season.

1.1 Deep- and Bottom-Water Formation

The northern North Atlantic (Greenland - Iceland - Norwegian (GIN) Sea) Ocean and the Labrador Sea are the major regions of North Atlantic Deep Water (NADW) formation (Clarke and Gascard, 1983; Aagaard and Carmack, 1994). The main mechanism is surface cooling under the background cyclonic circulation. Surface cooling of salty water in the GIN Sea and Labrador Sea produces relative warm and salty NADW (Carmack and Aagaard, 1973; Killworth, 1983). NADW flows southward along the east side of North and South America as a deep western boundary current. NADW enters the Antarctic Circumpolar Current (ACC) regime at about 45°S in the southwestern Atlantic and it is advected toward the east along the ACC (Reid and Lynn, 1971). Warm and salty Lower Circumpolar Deep Water (LCDW) which is located below Antarctic Surface Water slowly rises toward the surface of the Antarctic continental margin. Warm and salty Circumpolar Deep Water (CDW) may affect the sea ice to produce open area in sea-ice pack, a so-called open ocean polynya. Buoyancy loss through surface cooling (density increase) or freezing (brine release) can enhance convection and lead to a positive feedback in which a polynya can be maintained for several months (Martinson, 1990; Marsland and Wolff, 2001; Broecker, 1999). The Southern Ocean (SO) continental margin (predominantly the Weddell Sea, the Ross Sea, and off the Adélie Coast) (Jacobs et al., 1970; Gordon and Tchernia, 1972; Foster and Carmack, 1976) is the main region of Antarctic Bottom Water (AABW) formation (Brennecke, 1921; Mosby, 1934; Martinson, 1990; Gordon and Huber, 1990).

The coastal polynyas that are the open-water areas along the continental boundaries are the places where most new sea ice formation occurs by the persistent cold and strong katabatic winds that blow offshore being able to maintain the open-water areas. High Salinity Shelf Water (HSSW) created on the continental shelves due to a combination of sea-ice formation and accumulation mixes with LCDW along the continental slope. This mechanism is the case of near-boundary convection (Gordon 1998; Killworth 1983; Gill 1973; Foster and Carmack 1976; Jacobs et al. 1985; Whitworth et al. 1998; Jiang and Garwood 1995; Orsi et al. 1999). High density AABW produced in the Antarctic boundaries spreads up to the northern hemisphere, especially in the Atlantic (e.g. Reid, 1996), and competes with NADW in determining the global deep-ocean properties and circulation (e.g. Orsi et al., 1999).

1.2 Southern Ocean Sea Ice

Southern Ocean sea ice mainly consisting of thin first-year ice and being characterized by a huge seasonal cycle makes its simulation in global ocean General Circulation Models (GCMs) designed for long-term climate integrations a major challenge. Coupled atmosphere - ocean GCMs with present-day boundary conditions reveal large climate drifts in their deep-ocean properties after a few hundred years of global integration, mostly due to changes occurring in the models' formation rates of Antarctic Bottom Water (AABW)(e.g., Gordon et al., 2000). Higher-resolution (on the order of 80 km), regional sea-ice - ocean GCMs with focus on the Southern Ocean have undergone considerable progress over recent years (e.g. Timmermann et al., 2002), as has been verified mostly against satellite-derived passive-microwave data for ice concentration and extent. On a much coarser resolution (on the order of 200 km), this has also been attempted in long-term integrations with global sea-ice - ocean GCMs (e.g., Goosse and Fichefet, 1999; Duffy et al., 1999; Stössel et al., 2002), naturally with much less success, i.e. Southern Ocean sea ice in such integrations revealing substantial deficiencies (for coastal polynyas, see e.g. Stössel and Markus, 2004). This situation, of course, compromises the meaningfulness of such integrations when it comes to conclusions on regional or global climate change caused by long-term changes in the global thermohaline circulation, in particular when projected and linked to paleoclimatic conditions (e.g., Seidov et al., 2001; Kim et al., 1998).

1.3 Previous Model Studies

1.3.1 Coarse-Resolution Global Ocean GCM

Ocean GCMs typically used for climate studies and studies of the global thermohaline circulation use coarse resolution because they require long calculation time to reach steady state. A definition of steady state is every layer's global mean temperature variation being less than 0.01 degree per century and every layer's global mean salinity variation being less than 0.001 psu per century (England, 1993).

In case of bottom layer, it takes several hundred to thousand years to reach steady state. A coarse-resolution ocean GCM cannot resolve leads and polynyas which play a crucial role for deep-water formation. They are only represented in terms of the percent areal coverage or concentration of sea ice. I.e., leads and convection play a crucial role in deep- and bottom-water formation, but neither can be explicitly resolved in such models (including eddy-resolving GCMs). Both are thus in need of careful subgrid-scale parameterization. Selection of a "plume convection parameterization" instead of conventional "convective adjustment" is possible to represent deep penetration of small amount of surface water and shows more realistic asymmetric seasonal cycle of the Antarctic sea-ice area. Daily wind forcing has been employed in the Southern Ocean, in particular over sea ice, in order to capture leads that are typically created under the atmospheric synoptic variability, and would not emerge if monthly-mean winds were used. It also shows coastal polynyas along the Antarctic continental boundaries in form of reduced ice concentration (Stössel et al., 1998).

1.3.2 Several Attempts of High-Resolution Models

In order to describe open-ocean polynyas and coastal polynyas more accurately, high-resolution high-latitude models are necessary. Global high-resolution resolving eddy or plume convection ocean GCMs designed for studies of the long-term thermohaline circulation are not possible with present computer technology. An alternative approach would be to nest a high-resolution high-latitude model into a coarse-resolution global ocean GCM. Several regional Southern Ocean models are available for such purpose (e.g., Beckmann et al., 1999; Marsland and Wolff, 2001; Timmermann et al., 2002). Because they are regional models, the information of the global deep-ocean properties and thermohaline circulation is not available. While appealing at first glance, literature on nested models indicates still substantial technical problems, in particular when it comes to two-way nesting, it still has technical problems, such as momentum and heat at the boundary are not conserved (e.g., Spall and Holland, 1991; Fox and Maskell, 1996; Jacob and Podzun, 1997; Feser et al., 2001), which would need to work properly in long-term model integrations on the order of 1000 years.

A numerically more consistent alternative is using global curvilinear models with their poles over land close to regions that need higher resolution (Maier-Reimer, 1997; Mikolajewicz et al., 2001; Marsland et al., 2003). If the poles of the model are located near the boundary of sea and land of interest, the coastal polynyas that are important to produce deep and bottom water formation can be well represented. Unfortunately, in this type of model the time step must be reduced to keep the numerical stability by satisfying Courant-Friedrichs-Lewy condition, and is thus not suitable for long-term studies on changes of global deep-ocean properties.

A more recent verification of the performance of the high latitudes in a global sea-ice - ocean GCM includes the work of Timmermann et al. (2005). The highest resolution around Antarctica in their model is about 50 km. This is within a factor of 2 of the pixel resolution of the SMMR and SSM/I passive microwave data (Gloersen et al., 1992; Markus and Cavalieri, 2000), thus allowing for a fairly rigorous verification of modeled sea ice. In their verification, they include both polar regions as well as interannual variability, all based on monthly mean results. Their global integrations are restricted to 40 years, thus prohibiting conclusions about long-term changes of the global thermohaline circulation.

1.3.3 Ocean GCM Coupled to Atmospheric GCM

Another recent investigation of Southern Ocean sea ice in the framework of a global ocean GCM is that of Ogura et al. (2004), which is coarse resolution, but coupled to an atmospheric GCM. Since the atmosphere will respond to changes in sea ice, and vice versa, a half-way realistic simulation of Southern Ocean sea ice in such fully coupled framework is of course a much larger challenge. Indeed, the authors identify some major discrepancies between the coupled GCM and a forced stand-alone sea-ice model. Their coupled GCM was integrated for 200 years, the thermohaline circulation thus still featuring a transient state.

1.4 Objectives and Hypothesis

In order to keep the efficiency, ocean GCMs used for climate studies and studies of the global thermohaline circulation use coarse resolution. These do not resolve leads or polynyas. They show nevertheless quite reasonable deep- and bottom-water properties and global ocean circulation patterns, and even coastal polynyas along the continental boundaries in form of lower ice concentration. Subgrid scale convection schemes and ice concentration have been treated by giving certain empirical values, such as plume velocity or the radius of plume. The Hamburg Ocean Primitive Equation (HOPE) model used for this study is a global coupled sea ice - ocean model. This model uses same coarse grid sizes for both ocean and sea ice. The first objective of this study is a more accurate description of sea ice by enhancing the resolution of the sea ice grid to represent the deep- and bottom-water properties and global thermohaline circulation pattern more realistically by more detailed sea-ice - ocean interactions and more accurate coastal and open-ocean polynyas, thus providing the ocean with more realistic buoyancy fluxes.

The second objective is to test the validity of the empirical data used in long-term integrations. If both coarse- and fine-grid sea-ice grids show reasonable deep- and bottom-water properties and global circulation pattern with same empirical values, the values can be considered reasonable values for other sizes of sea-ice grid. But if fine sea-ice grid with same empirical values shows unreasonable deep- and bottom-water properties or global circulation pattern, reasonable values of empirical data need to be chosen. To achieve these objectives, this study will:

a) investigate the impact of the surface buoyancy fluxes that are now refined due to the higher-resolution sea-ice grid, which is coupled to the coarse global ocean GCM,

b) analyze what makes the difference between coarse grid and fine grid sea ice for the deep- and bottom-water properties and global thermohaline circulation,

c) investigate and analyze the effect of fine-grid (same size of fine sea-ice grid) of plume convection parameterization.

In the first step, the impact of deep- and bottom-water temperature and salinity, ice concentration along the continental margin, ice thickness, the quantity of thermohaline circulation at some key points, and convective potential energy release due to enhance the sea-ice resolution will be investigated. These experiments will be reported in Chapter III.

In the second step, a further enhancement of the resolution of the sea-ice model brings its grid size to about 22 km, i.e., the same size as that of the satellite passive microwave sensors SMMR and SSM/I (e.g., Gloersen et al., 1992; Markus and Cavalieri, 2000) from which sea-ice concentration is routinely retrieved. These are used in this study to directly compare with the simulated ice concentration. These experiments will be reported on in Chapter IV.

Chapters II-V are organized as follows. Chapter II describes the sea-ice - ocean climate model employed in this study, including the boundary conditions to drive the model by the atmosphere. Chapter III describes the study of 9-fold higher-resolution sea ice coupled to the coarse sea-ice grid, the main results of which have been published in Stössel and Kim (2006). Chapter IV describes experiments of sea ice in long-term global ocean GCM integration with an additional 9-fold enhanced resolution of sea ice and convection. The overall conclusions of this dissertation will be given in Chapter V.

CHAPTER II

MODEL CONFIGURATION

The "Hamburg Ocean Primitive Equation" model, HOPE, is an ocean general circulation model (OGCM) based on the primitive equations with representation of dynamic-thermodynamic processes of sea ice. For the long integration time to reach steady state of the deep ocean, only coarse- resolution GCMs are feasible for long- term sensitivity studies (Hirst and Cai, 1994; Danabasoglu and McWilliams, 1995; Toggweiler and Samuels, 1995; Hu, 1997; Large et al., 1997; Duffy and Caldeira, 1997, etc.). High-resolution models can reproduce important small-scale features such as eddies and convection. However, due to computational constraints, long-term deep ocean studies and global coupled atmosphere-ocean climate modeling studies will for the next generation of models still be undertaken with coarse-resolution ocean components (Delworth et al., 1993; Manabe and Stouffer, 1996; Washington and Meehl, 1996, etc), i.e., without resolving eddies, and in particular without resolving convective plumes.

2.1 Oceanic Component

HOPE is based on the primitive equations with a prognostic free surface, the non-linear balance equation, the hydrostatic and Boussinesq approximations for momentum, the continuity equation for an incompressible fluid, and conservation equations for heat and salt. Prognostic ocean variables are horizontal velocities $\vec{v}$, sea-surface elevation ζ , potential temperature θ , and salinity S . The baroclinic pressure p is calculated from the hydrostatic equation. The equation of state calculates density from T, S and p. The Boussinesq approximation implies a constant density in the x- and y-component of the momentum equation. The model adapts the local topography for the lowest column. The grid is discretized using an Arakawa E-grid (Arakawa and Lamb, 1977) which is identical to the "B" grid rotated by 45 degrees. The HOPE model employed in this study has horizontal resolution of 3.5° X 3.5° and 11 unevenly spaced vertical layers for oceanic part and a time step of 20 hours (Wolff et al., 1997).

Crucial for the coupling of the atmospheric fields to the ocean is the detailed surface heat balance calculation, which features a subgrid distinction between the open-water and ice-covered part of a model grid cell. The overall heat flux per grid cell is thus a direct function of the modeled ice concentration. In order to capture leads created by atmospheric synoptic processes, the wind forcing over the Southern Ocean is provided by daily analyses fields of the European Centre for Medium Range Weather Forecasts (ECMWF) of one year. Otherwise, the momentum, heat and fresh-water flux are based on monthly climatological fields (see Drijfhout et al., 1996). Furthermore, the model includes a subgrid-scale plume convection parameterization following Paluszkiewicz and Romea (1997) (Kim and Stössel, 2001).

The momentum equations include parameterizations for horizontal and vertical turbulent viscous momentum dissipation $\vec{F}_H$ and $\vec{F}_V$:

$$\frac{d}{dt}\vec{v} + f(\vec{k} \times \vec{v}) = -\frac{1}{\rho_0}(\vec{\nabla}_H(p + \rho_0 g\zeta)) + \vec{F}_H + \vec{F}_V .$$

$\vec{v} = (u,v)$ is the horizontal velocity vector, f the Coriolis parameter, $\vec{k}$ the upward vertical unit vector, ρ_0 a constant reference density, g the acceleration due to gravity. The total derivative reads

$$\frac{d}{dt} = \frac{\partial}{\partial t} + \vec{v} \cdot \nabla_H + w \cdot \frac{\partial}{\partial z} ,$$

where ∇_H is the horizontal gradient operator. The horizontal viscous dissipation $\vec{F}_H$ is composed of a term depending on the local rate of strain and of harmonic and biharmonic background terms:

$$\vec{F}_H = \nabla(v_A T^2 \vec{\nabla}_H(\vec{v})) + A_H \nabla^2(\vec{v}) - B_H \nabla^4(\vec{v}) ,$$

where A_H, B_H, and v_A are constant coefficients, ∇ the gradient operator, $\nabla^2 = \nabla \cdot \vec{\nabla}_H$ the horizontal Laplace operator, and T^2 a function of the local rate of strain $\partial v/\partial x + \partial u/\partial y$.

The vertical eddy viscosity is parameterized as

$$\vec{F}_V = \frac{\partial}{\partial z}(A_V \frac{\partial}{\partial z}\vec{v}) \ ,$$

where the eddy coefficient A_V can be specified to depend on the local Richardson number. The internal pressure p is related to the density field by the hydrostatic equation

$$\frac{\partial p}{\partial z} = -g\rho \ .$$

The vertical velocity w is calculated diagnostically from the incompressibility condition

$$\frac{\partial w}{\partial z} = -\nabla_H \cdot \vec{v} \ .$$

The sea-surface elevation is calculated from the linearized kinematic boundary condition

$$\frac{\partial \varsigma}{\partial t} = w\big|_{z=0} + Q_\zeta = -\nabla \int_{-H}^{0} \vec{v} dz + Q_\zeta \ ,$$

where $H(x,y)$ is the water depth, and Q_ζ the fresh-water forcing at the free surface.

Salinity S and potential temperature θ are determined from the continuity equations

$$\frac{dS}{dt}=\frac{\partial}{\partial z}\left(D_v\frac{\partial S}{\partial z}\right)+D_H\nabla^2(S)+\nabla\left(v_D T^2\vec{\nabla}_H(S)\right)$$

$$\frac{d\theta}{dt}=\frac{\partial}{\partial z}\left(D_v\frac{\partial \theta}{\partial z}\right)+D_H\nabla^2(\theta)+\nabla\left(v_D T^2\vec{\nabla}_H(\theta)\right)$$

where v_D and D_H are constant coefficients, and T^2 is defined as for the horizontal viscosity. The vertical eddy diffusivity D_v can be specified to depend on the local Richardson number.

2.2 Sea-Ice Component

The model includes a comprehensive dynamic-thermodynamic sea-ice model (Stössel and Owens, 1992). It is based on the formulations given in Hibler (1979) and Owens and Lemke (1990). The sea-ice dynamics employ the viscous-plastic constitutive law of Hibler (1979) to describe the internal ice stress. The sea-ice momentum equation is:

$$\frac{d\vec{v}_i}{dt}=-f\vec{k}\times\vec{v}_i+\frac{\vec{\tau}_a}{\rho_i h_i}+\frac{\vec{\tau}_o}{\rho_i h_i}+\frac{\vec{F}_i}{\rho_i h_i}-g\bullet\nabla_H\zeta$$

where $\vec{v}_i$ is the two dimensional ice velocity, $\vec{\tau}_a$ the stress at the atmospheric interface, $\vec{\tau}_o = -\vec{\tau}_i$ the ice-water stress. $\vec{F}_i$ is the force due to variations of internal ice stress and determined from $\vec{F}_i = \frac{\partial \sigma_{ij}}{\partial x_j}$.

ρ_i and h_i are the ice density and the (grid-cell) mean ice thickness.

As in Hibler (1979), the internal ice stress is modeled in analogy to a non-linear viscous compressible fluid obeying the constitutive law

$$\sigma_{ij} = 2\eta\dot{\varepsilon}_{ij} + (\zeta - \eta)\dot{\varepsilon}_{kk}\delta_{ij} - \frac{P\delta_{ij}}{2}$$

where σ_{ij} is the two-dimensional stress tensor, $\frac{P}{2}$ an ice-pressure term, and ζ and η non-linear bulk and shear viscosities.

The dynamics and thermodynamics are linked by the continuity equations for ice thickness, ice compactness, and snow depths:

$$\frac{\partial h_i}{\partial t} = -\nabla \bullet (\vec{v}_i h_i) + \left(\frac{\partial h_i}{\partial t}\right)_{th} + diffusion\ ,$$

$$\frac{\partial N_i}{\partial t} = -\nabla \bullet (\vec{v}_i N_i) + \left(\frac{\partial N_i}{\partial t}\right)_{th} + diffusion\ ,$$

$$\frac{\partial h_{sn}}{\partial t} = -\nabla \bullet (\vec{v}_i h_{sn}) + \left(\frac{\partial h_{sn}}{\partial t}\right)_{th} + diffusion\ ,$$

where N_i is the ice compactness, and h_{sn} is the mean snow thickness, and the index th represents thermodynamic terms.

The heat balance equation has two forms, one for the ice-free and one for the ice-covered part of a model grid cell, following Semtner (1976) and Parkinson and Washington (1979). The surface heat flux Q_w over the ice-free part of the grid cell, is calculated using a heat balance equation

$$Q_w = (1-\alpha_w)Q_s + Q_l - \varepsilon_w \sigma T_w^4 + Q_{lat} + Q_{se} ,$$

where T_w is the upper ocean temperature. Q_s and Q_l are the incident shortwave and longwave radiation heat fluxes, Q_{lat} and Q_{se} are the latent and sensible turbulent heat fluxes over the water. α_w and ε_w are the albedo and thermal emissivity of the sea surface.

Over the ice-covered part of a grid cell, a similar heat budget including the conductive heat flux (Q_c) through the snow/ice layer is:

$$0 = (1-\alpha_i)Q_s + Q_l - \varepsilon_i \sigma T_i^4 + Q_{lat} + Q_{se} + Q_c \equiv Q_a + Q_c$$

where Q_s and Q_l are the incident shortwave and longwave radiation heat fluxes, Q_{lat} and Q_{se} are the latent and sensible turbulent heat fluxes over the snow or ice surface. T_i is the ice temperature. α_i and ε_i are the albedo and thermal emissivity of the snow or ice surface.

2.3 Higher-Resolution Sea-Ice Model

A global coarse-resolution version of the HOPE model is the starting point for the new model setup. This version is identical to that described in Stössel et al. (2002), which is a majorly revised offspring of the version of Drijfhout et al. (1996).

As a first attempt of a higher-resolution sea-ice model "nested" in a coarse-resolution ocean model, the sea-ice model’s resolution is enhanced by a factor of 9, i.e. each (upper-layer) ocean grid point is coupled to 9 sea-ice grid points. The way this is realized on the Arakawa E-grid of the model is illustrated in Figure 1. This

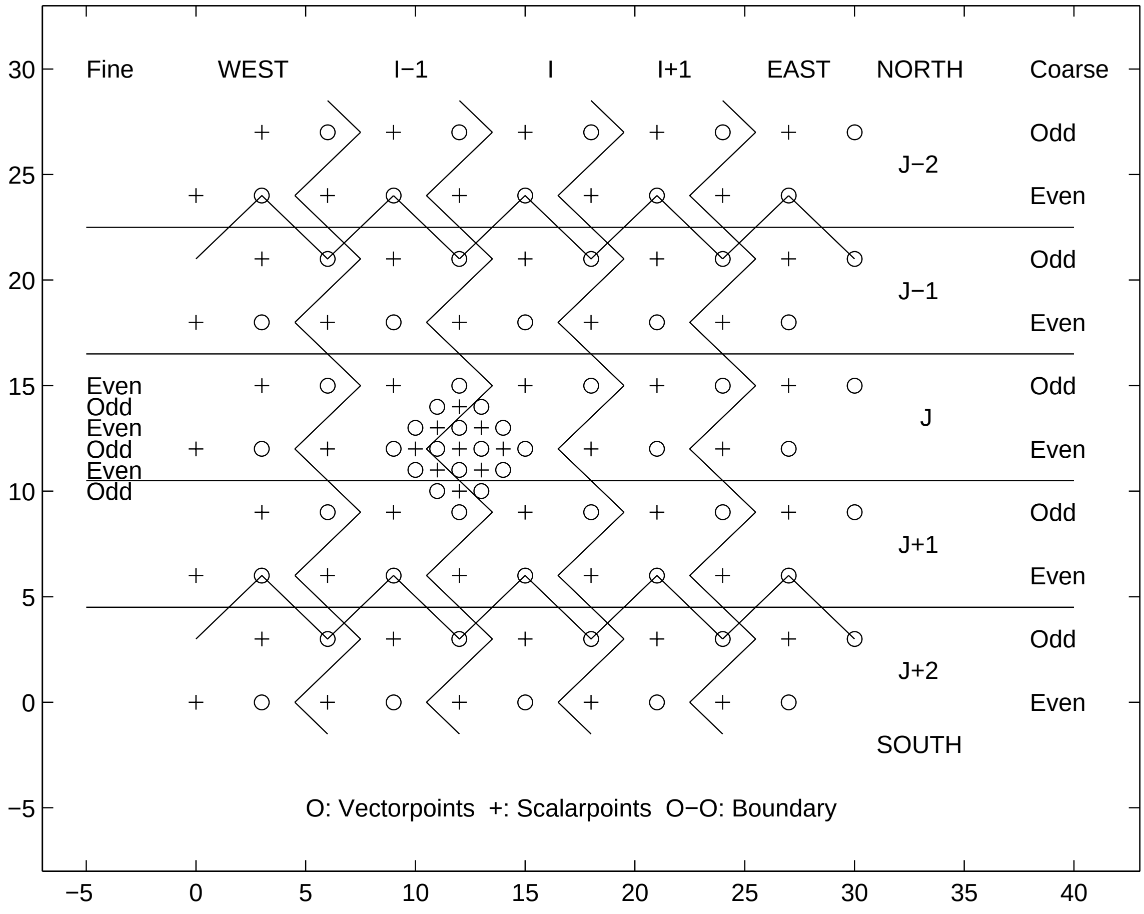

Figure 1. 9-fold resolution enhancement in Arakawa E-grid. The embedded finer resolution of the sea-ice component is shown for the coarse even scalar point I, J. The underlying graph is from Wolff et al. (1997).

procedure reduces the grid spacing approximately from 200 km to 80 km. This is applied only in the southern hemisphere south of 50S, north of which sea ice does normally not occur (Gloersen et al., 1992), and the reason it is not applied to the whole ocean has been explained in Chapter I. In order to avoid artificial abrupt gradients across coarse grid-cell borders, all atmospheric forcing fields are smoothed over 9 fine grid points, respectively. All relevant oceanic fields are converted from the coarse to the fine grid each time step before sea ice is integrated forward. This procedure involves smoothing of the ocean currents and the sea-surface height (which is a prognostic quantity in the ‘free-surface’ ocean GCM used here). Each time step the prognostic sea-ice calculation is completed, its impact on the ocean requires a conversion of the affected ocean variables to the coarse grid, which involves a simple averaging procedure. Note that in order to preserve their fine-grid properties during the prognostic time-stepping, the sea-ice variables are not subject to this conversion procedure.

While the conversion described above enhances the resolution of the ocean GCM’s sea-ice component, the ocean is still calculated on the coarse grid, which implies that the coastline (around Antarctica) is limited in its resolution by the coarse grid. This leads to artifacts along the coastline that may reduce the benefits of simulating sea ice with higher resolution along the coast. In particular, the locations of the coastal polynyas may not be represented all that much more realistic with the higher resolution model than with the coarser resolution one. To improve this situation, an additional model version ("CFF") has been created in which the coastal ocean grid columns are partially being covered at their surface following the finer ice shelf/land margin of satellite-derived passive microwave data (in particular the Special Sensor Microwave Imager, SSM/Is e.g., Markus and Cavalieri, 2000). This cover is specified to essentially inhibit any momentum, heat, and fresh-water flux between atmosphere and ocean by specifying it as fast ice with a thickness of 10 meter. This procedure required a prior "excavation" of coarse-grid coastal grid points where the SSM/I data shows sea ice or open water and the coarse model land. Conversely, ocean grid points were filled where they are entirely within the SSM/I boundary. Since the center of the new wet grid points is geographically located over land, these points had to be provided with a water depth, which was chosen to be 450 m. Note that because of the change in the number of wet points, the results of the new equilibrium integration feature changes in the ocean’s circulation and properties that are not solely due to the finer sea-ice coastline.

For the experiments described in Chapter IV, the technique of the 9-fold resolution enhancement has been repeated in a straightforward successive manner by increasing the resolution of the 9-fold enhanced grid another 9-fold to arrive at the 81-fold enhanced grid. Otherwise, the procedure is similar to the previous step. In a further enhanced version of the model, where the one-dimensional plume convection parameterization is run on the same grid as the sea-ice component, fine-grid temperature and salinity anomalies are preserved during the integration. With this approach, the fine-grid structure of the temperature and salinity fields is more consistent with the fine-grid sea-ice fields, which are entirely preserved on the fine grid during the model integration.

In order to capture coastal polynyas geographically as accurately as possible, the model’s Antarctic ‘coastline’ for the sea-ice module has been determined by the fine-grid satellite passive-microwave demarkation line between ice-free or ice-covered ocean and land or ice shelf. This assumption is consistent with the "CFF" case described above. Furthermore, it provides the option of "ice-shelf melt", the effects of which have been investigated in Stössel et al. (2007).

CHAPTER III

9-FOLD HIGHER RESOLUTION OF SEA ICE IN LONG-TERM GLOBAL OCEAN GCM INTEGRATIONS*

High-latitude surface conditions are to a large extent controlled by the presence of sea ice, in particular by processes associated with its formation and melting, and its drift and dynamic compression. Of particular importance is the occurrence of leads and polynyas (e.g., Comiso and Gordon, 1998; Markus et al., 1998; Eisen and Kottmeier, 2000; Goosse and Fichefet, 2001; Renfrew et al., 2002). These can be a product of divergent ice drift, either near the shore line or in the open ocean, or of oceanic heat flux, e.g. in conjunction with convective plumes.

---

* Partially reproduced from "Enhancing the Resolution of Sea Ice in a Global Ocean GCM" by Achim Stössel and Joong-Tae Kim, 2006. Ocean Modelling, 11, 28-48, with permission by Elsevier 2007.

Ocean GCMs are unable to resolve leads and polynyas. Rather, such are parameterized as open-water fraction per grid cell of a sea-ice model that is coupled to the ocean GCM (e.g., Marsland et al., 2003). Higher resolution (sea-ice) - ocean GCMs would be a logical step toward a more detailed representation of open water in the ice pack. This, however, is not feasible because of the long deep-ocean adjustment time which constrains an ocean GCM designed for thermohaline circulation studies to coarse resolution (see Chapter I). A compromise is presented in which the resolution of merely the sea-ice component is enhanced, thereby refining the representation of leads and polynyas, while retaining the ocean model efficient enough to conduct investigations on the impact of high-latitude processes on global deep-ocean properties and circulation.

Enhancing the sea-ice grid from 200 km to 80 km is an intermediate step toward a resolution of 22 km, which is close to the pixel resolution of satellite passive microwave data from which ice concentration is routinely derived (Gloersen et al., 1992; Comiso, 1995; Markus and Cavalieri, 2000). The final step is to allow for a rigorous evaluation of the simulation of sea ice in a global ocean GCM, sea ice acting as a sensitive gauge for the quality of the global simulation. This study is to demonstrate that global simulations with a ‘nested’ higher-resolution sea-ice component are robust and promising enough to envision the next step of resolution enhancement. Given the fact that leads and polynyas occur in locations of most vigorous heat loss in fall and winter, a higher-resolution sea-ice component is also worthwhile to be aimed at in view of a coupling with the atmosphere. The approach presented here might thus also become useful for the next generation of coupled climate GCMs.

The objective of the research described in this chapter is to investigate which aspects produce the differences between the coarse-grid sea ice and higher-resolution sea ice. To compare with the same coarse coastline, the results from the coarse ocean - coarse sea ice - coarse coastline (CCC) model are compared with those from the coarse ocean - fine sea ice - coarse coastline (CFC) model. Subsequently, the results of coarse ocean - fine sea ice - fine coastline (CFF) model (see Chapter II) are compared to the CFC model. All model results shown represent cyclostationary equilibrium solutions attained after global model integrations on the order of 1000 years.

3.1 Experiments and Results

3.1.1 CCC versus CFC

Figure 2 shows ice concentration as September mean (a), a mid-September (b), and ice thickness of September mean (c) of the results of simulation CCC. Ice concentration of September was chosen to be compared because September has its maximum ice extent. Figure 3 is the results of CFC, which use fine sea-ice grid. For the direct comparison with CCC results, they are represented on the coarse grid. Both September mean ice concentrations (2-a, 3-a) do not look

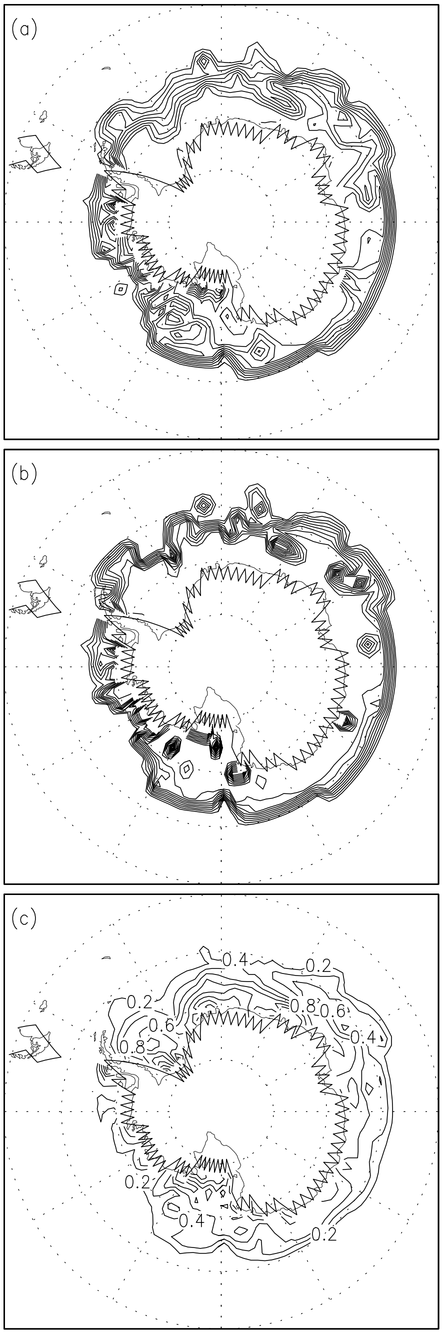

Figure 1. September mean (a) and mid-September (b) ice concentration, as well as September mean ice thickness (c) as simulated with CCC (see text). The isolines of ice concentration range from 10 % to 100 % with an increment of 10 %. Thickness increment is 0.2 m.

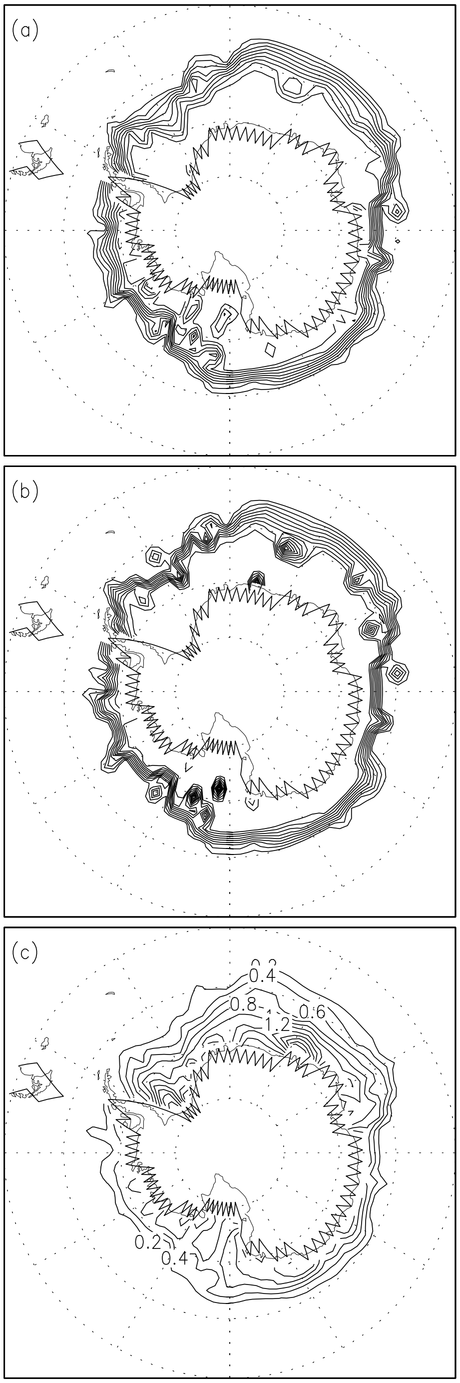

Figure 2. September mean (a) and mid-September (b) ice concentration, as well as September mean ice thickness (c) as simulated with CFC, displayed on coarse grid.

realistic comparing to the satellite-derived data (Figure 4). CFC has larger extent in the Indian Ocean sector which is more close to nature. In both experiments, the ice extent of the Weddell Sea is underestimated.

The openings (polynyas) in the ice pack due to the plume convection in daily snapshots appear sporadically and maintain for a few days until the phase of "lateral exchange" (Marshall and Schott, 1999) sets in and the water column gradually retains stable stratification. CCC has overestimated polynyas. CFC corrects this a little bit but still overestimates polynyas when compared to the satellite-derived ice distribution.

The fine-grid sea-ice integration shows its maximum benefits when it is represented on its own fine grid. Figure 5 is the fine-grid ice concentrations (5-a, 5-b) and ice thickness (5-c) of CFC. The most striking difference to the CCC is its sharp ice edges and openings along the coastline. These are more realistic when compared to the

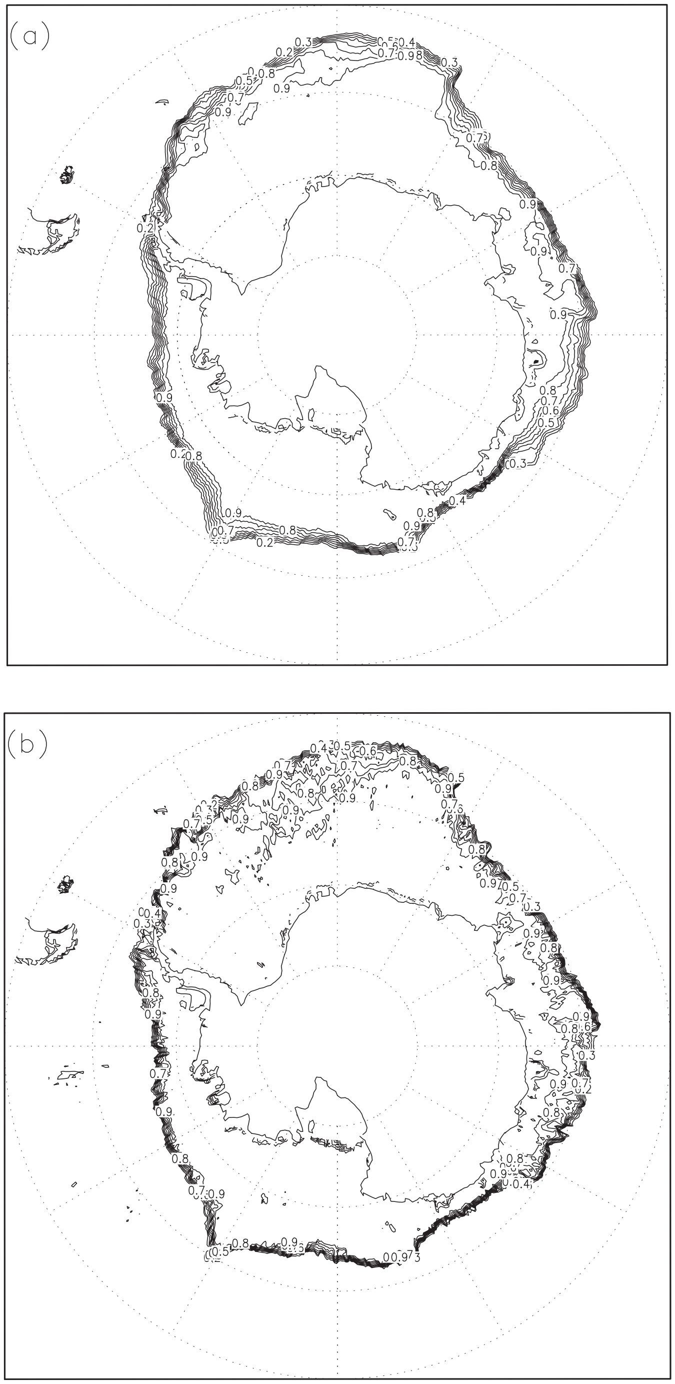

Figure 4. Year 1992 September mean (a) and mid-September (b) ice concentration, as derived from SSM/I data using the NASA Team 2 algorithm, displayed at the highest available resolution (about 22 km).

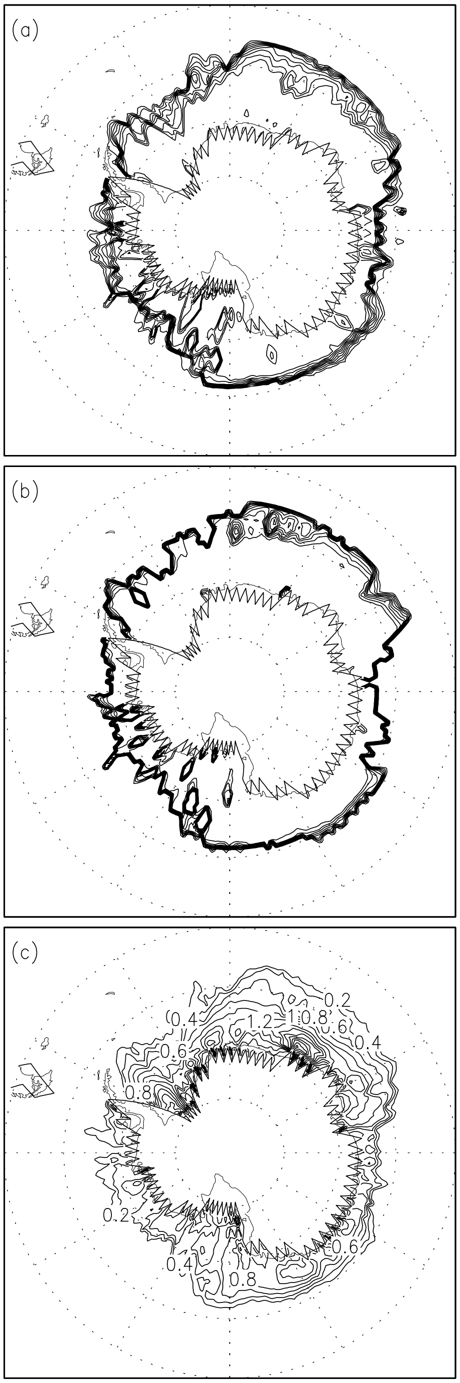

Figure 5. September mean (a) and mid-September (b) ice concentration, as well as September mean ice thickness (c) as simulated with CFC, displayed on fine grid.

satellite-derived data (Figure 4). The ice thickness represents more details, which is understandable because the sea-ice dynamics such as nonlinear ridging that occur under compression are simulated on the fine grid.

In terms of long-term, global impacts of refinement of sea ice in Southern Ocean, some choke point numerical data are listed in Table 1 (CCC versus CFC). There is a slight reduction of NADW outflow across 30 S in Atlantic (0.6 Sv) and Drake Passage throughflow by 8 Sv. The deep ocean annual and global mean of 4000 m potential temperature becomes slightly cooler (0.13 degree) and salinity becomes fresher (0.026 psu) with the higher sea-ice resolution. These results give the clue that high-resolution sea-ice model produce more AABW formation through enhanced near-boundary convection.

Table 1. Selected annual mean choke point numbers of the thermohaline circulation for the listed experiments (abbreviations explained in text)

Exp.	NADW [Sv]	DP [Sv]	θ_{4000m}[degC]	S_{4000m}[psu]
CCC	12.1	105	1.43	34.746
CCC/V	11.1	108	1.26	34.750
CCC/L	10.7	112	1.11	34.749
CCC/CP	11.3	110	1.26	34.747
CCC/K	11.1	107	1.15	34.730
CFC	11.5	97	1.30	34.720
CFC/V	11.1	99	1.25	34.732
CFF	10.5	81	0.56	34.657

NADW outflow is the southward flow of NADW across 30 °S in the Atlantic. DP stands for Drake Passage (the throughflow through which is a measure for the strength of the ACC). θ_{4000m} and S_{4000m} represent the global mean potential temperature and salinity at 4000 m depth, respectively.

3.1.2 CFC versus CFF

While these dynamic features along the coastline are better captured with the higher resolution, the pattern is rather unrealistic since the coastline is dictated by the coarse grid. The artificial bays may due to the Arakawa E-grid in conjunction with spherical latitude-longitude coordinates, but this would be an issue with any other non-curvilinear, spherical grid. To improve this situation, an additional model version has been created in which the coastal ocean grid columns are partially being covered at their surface following the finer ice shelf/land margin of satellite-derived passive microwave data (in particular the Special Sensor Microwave Imager, SSM/I; e.g., Markus and Cavalieri, 2000). This cover is specified to essentially inhibit any momentum, heat, and fresh-water flux between atmosphere and ocean by specifying it as fast ice with a thickness of 1 meter. This procedure required a prior "excavation" of coarse-grid coastal grid points where the SSM/I data shows sea ice or open water and the coarse model land. Conversely, ocean grid points were filled where they are entirely within the SSM/I boundary. These mentioned above are the experiment CFF. The original coarse coastline, the newly "excavated" coarse coastline, and the new fine SSM/I-based "coastline" are illustrated in Figure 6.

The results of CFF experiment are shown in Figure 7. The sharp ice edge and much details on ice thickness distribution on CFF (Figure 7) are similar to the experiment CFC (Figure 5). The pattern of ice extent has changed, ice extent at the Weddell Sea section is more realistic than CFC comparing to the satellite data (Figure 4). Ice thickness in the Weddell Sea section is much more realistic comparing to the upward-looking sonars (Strass and Fahrbach, 1998; Harms et al., 2001).

Comparing global ocean properties and the thermohaline circulation, CFF to CFC, the annual and global mean potential temperature of CFF at deep ocean has cooled and its salinity becomes fresher. The NADW outflow of CFF has significantly reduced as well as DP throughflow in

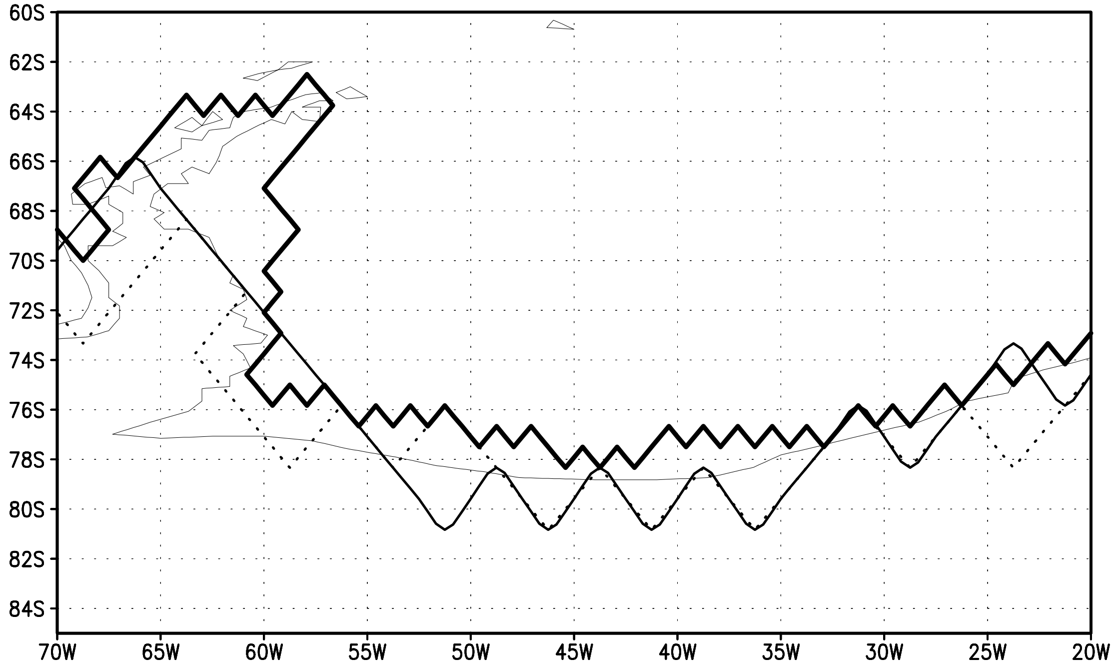

Figure 6. Coastline representation of the original coarse grid (thin solid line), the excavated grid where it differs from the original grid (dotted line), and the SSM/I-derived grid (thick solid line).

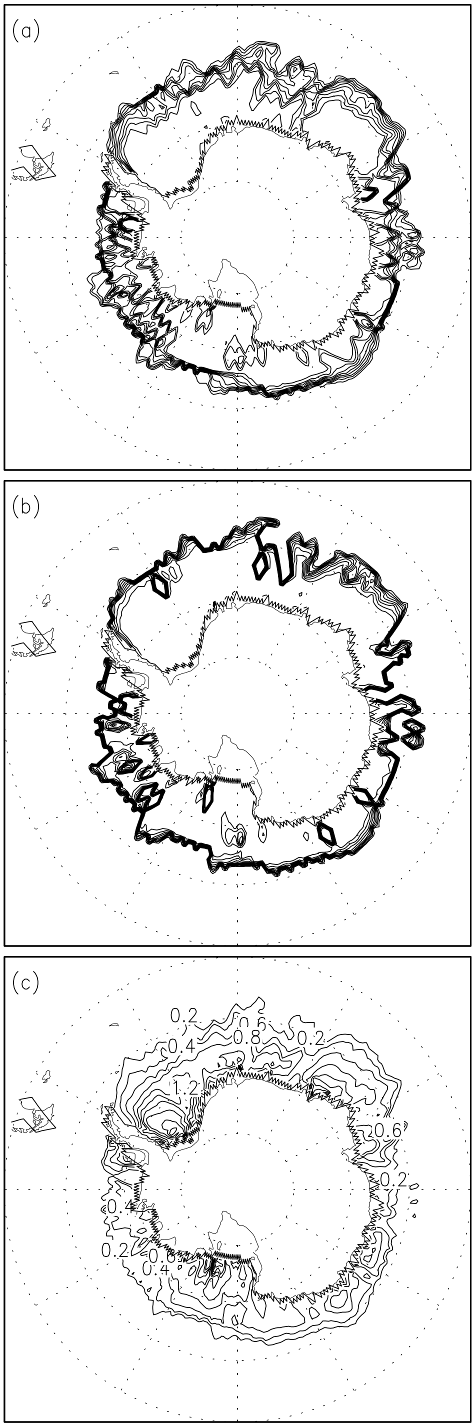

Figure 7. September mean (a) and mid-September (b) ice concentration, as well as September mean ice thickness (c) as simulated with CFF, displayed on fine grid.

terms of Antarctic Circumpolar Current (ACC). These evidences indicate that AABW formation of CFF is more dominant in the world’s ocean, and suggest a considerably reduced density gradient across the ACC. The tendency of CFC to CFF goes in the same direction as CCC to CFC, only that they are much stronger than the former.

Further details of the ice-thickness distribution achieved with CFF can be identified in Figure 7-c versus Figure 5-c. Excessive ice thickness in the bays along the coastline of the Weddell Sea and Adélie Coast of CFC has significantly vanished in CFF. Figure 8 shows the details of ice thickness and ice velocity in Weddell Sea. Since coastal polynyas are the regions where most brine is formed, an enhanced resolution of their model representation is essential if the global properties and circulation of the deep ocean are to be captured realistically in a global model. It is also obvious that a further enhancement of the resolution is desirable.

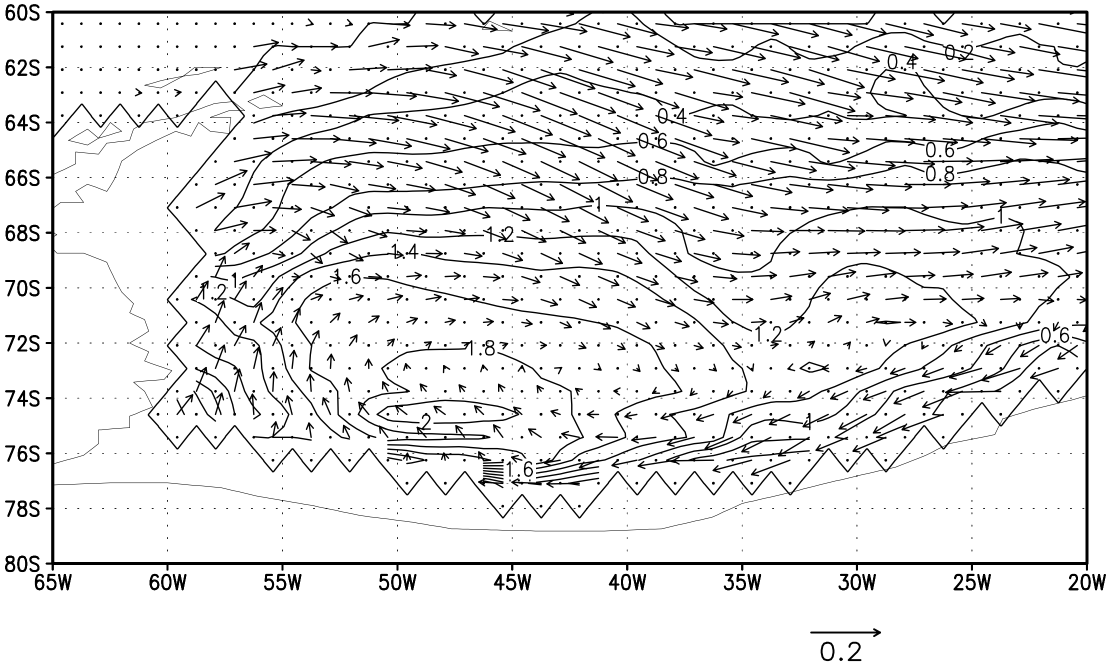

Figure 8. September mean ice thickness and velocity in the western Weddell Sea as simulated with CFF. The ice-thickness increment is 0.2 m. The reference arrow represents 0.2 m/s.

3.2 Discussions

The aim of the sensitivity experiments in this chapter is to explore the differences between CFC and CCC as listed in Table 1. One expectation of enhancing the sea-ice resolution is that an overall larger lead fraction will emerge in fall and winter where the ice concentration is high and where it decisively determines the heat flux. Figure 9 shows the average ice concentration in fall and winter in the range of 90-100 % south of 60 S. As it is expected, the ice concentration of CFC is always smaller than that of CCC, by up to 3 %, in particular during the fall when the ice starts to freeze.

Figure 10 shows the differences of temperature and salinity as annual and zonal average (between 60 W and 20 E) for the Atlantic Ocean. From the CFC value CCC value is subtracted. Besides the deep water being cooler and fresher known from Table 1, several other features can be explained. At the Antarctic continental margin and to the 4000 m at 60 S being cold and fresh, that is due to more AABW formation by

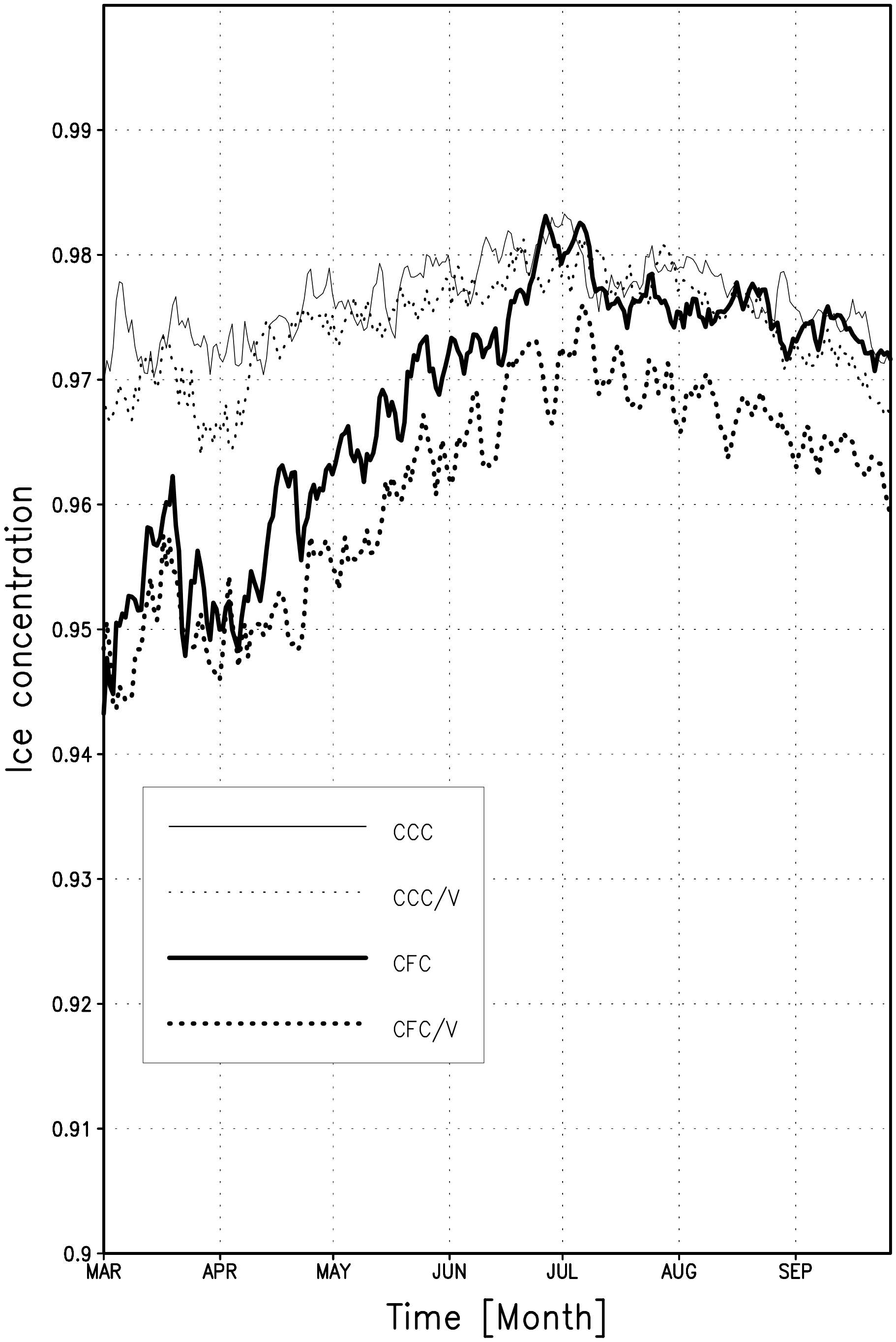

Figure 9. March-September ice concentration south of 60 S for where and when it is in excess of 90 % for simulations as indicated (see text).

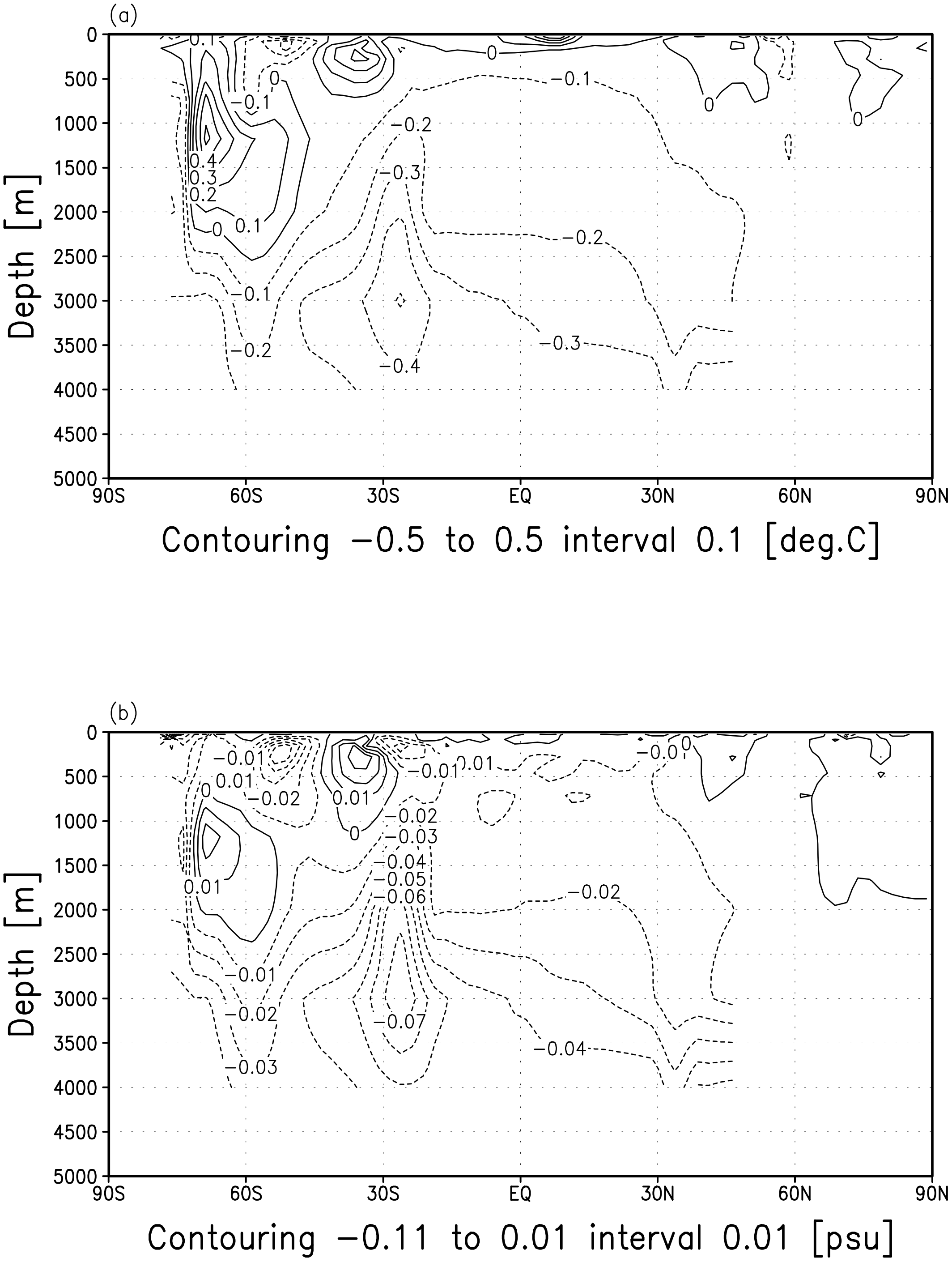

Figure 10. Difference of Atlantic annual and zonal mean potential temperature (a) and salinity (b), CFC minus CCC.

increasing near-boundary convection with less CDW entrainment. Between 1500 m to 3500 m at 25 S, CFC is colder and fresher than CCC. The enhanced northward intrusion of AABW across 30 S reduces NADW outflow, a correlation that has been noticed and discussed in earlier studies (e.g., Seidov et al., 2001; Stössel and Kim, 2001; Stössel et al., 2002). Warmer and saltier at 70 S between 500 m and 2000 m reflects more pronounced CDW signal due to less open-ocean convection. Figure 11 shows the potential energy release that is consistent with plume convection reduction explained in section 3.1. As a result of the stronger stratification in the open-ocean part of the Weddell Sea, a more pronounced Antarctic Intermediate Water (AAIW) signal is in 1000 m depth at 55 S by more freshwater retaining in the surface layer. The warming south of 60 S is reducing the meridional density gradient across the latitude of ACC, thus reducing its strength.

To find what mechanism makes the difference between CCC and CFC, some additional experiments have been conducted. Since sea ice directly

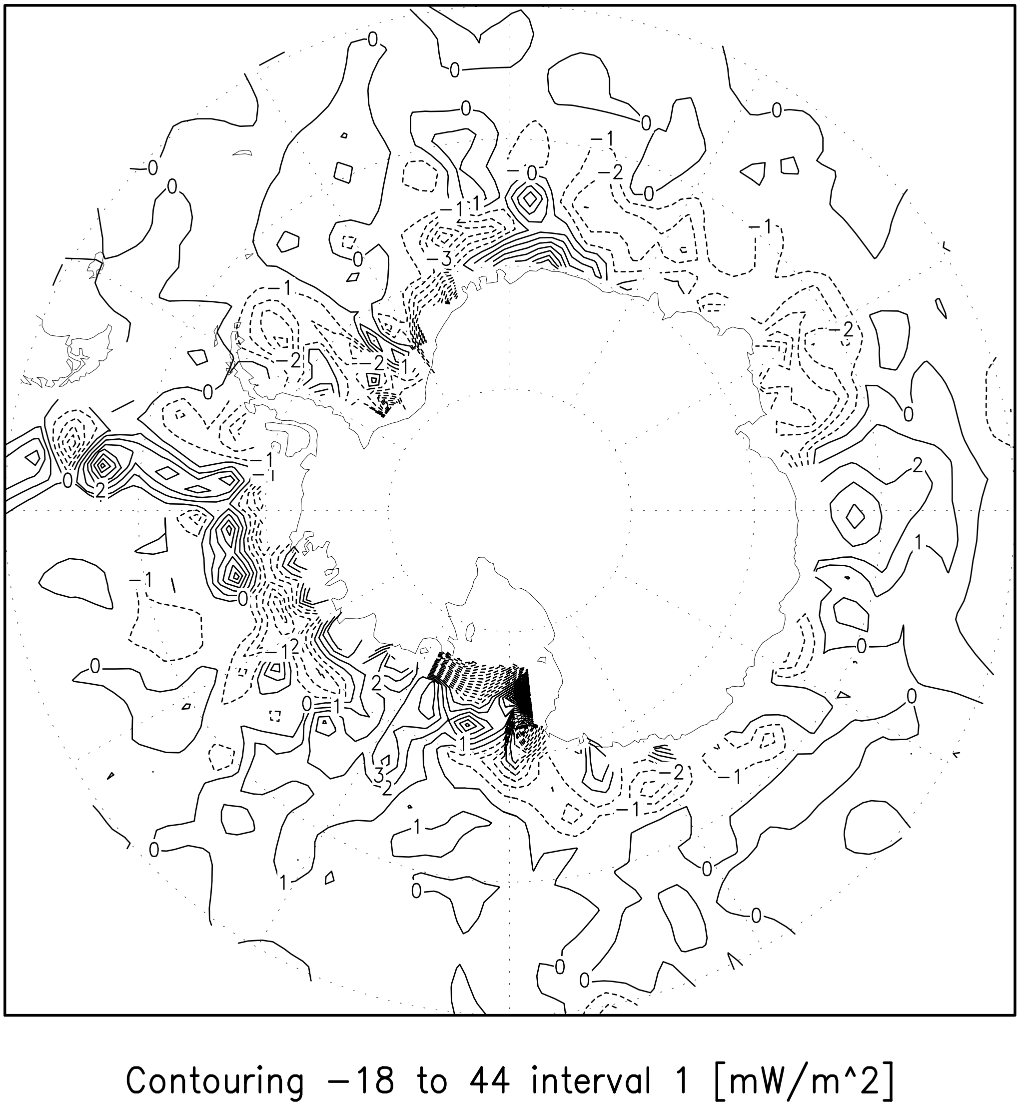

Figure 11. Difference in annual mean convective potential energy release, CFC minus CCC.

responds dynamically mainly to the wind as opposed to the currents, one might expect that high-resolution sea ice is largely affected by the high-resolution wind forcing. Therefore, the wind variability experiment (CCC/V) has been conducted (Table 1). To enhance the wind variability, 0.06 N/m^2 is added to the zonal wind-stress component in every other vector points in zonal direction, and the same amount subtracted, at the respective grid points in between. Not only spatial variability but also temporal variability is considered: every time step the direction is reversed to maximize the variability. This experiment is to induce more opportunities for the sea-ice pack to converge and diverge with the expectation to produce more leads, as is common in nature, e.g. in conjunction with the passage of weather fronts or with tidal currents (e.g., Padman and Kottmeier, 2000). It can represent more detail of producing ridges by converging and leads by diverging when the model uses high-resolution of wind forcing and sea-ice component. The dotted lines in Figure 9 show the effect of variability on ice concentration in a range 90-100

%. From fall to winter both CCC and CFC experiments, the enhanced wind variability produces 0.5 to 1 % more open water.

The enhanced wind variability leads to similar tendencies in both coarse and the fine sea-ice model versions (i.e., CCC versus CCC/V and CFC versus CFC/V) (Table 1). In CCC/V, deep water changes slightly cooler (0.17 degree versus CCC) and saltier (0.004 psu). This is in conjunction with slight increase of Antarctic Circumpolar Current (ACC) (by 3 Sv) and reduction of NADW outflow (by 1 Sv). This is due to enhanced AABW formation not because of the near-boundary convection but of the open-ocean convection. CFC has more AABW formation due to the near-boundary convection than CCC. The meridional section comparison of CCC and CCC/V (Figure 12) shows different pattern from CFC and CCC (Figure 10). Southern Ocean south of 60 S is colder in CCC/V than what resulted with CFC. Deep ocean in CCC/V becomes overall denser and the density across the ACC increase due to waters south of the ACC becoming less stratified and denser because of enhanced open-ocean convection.

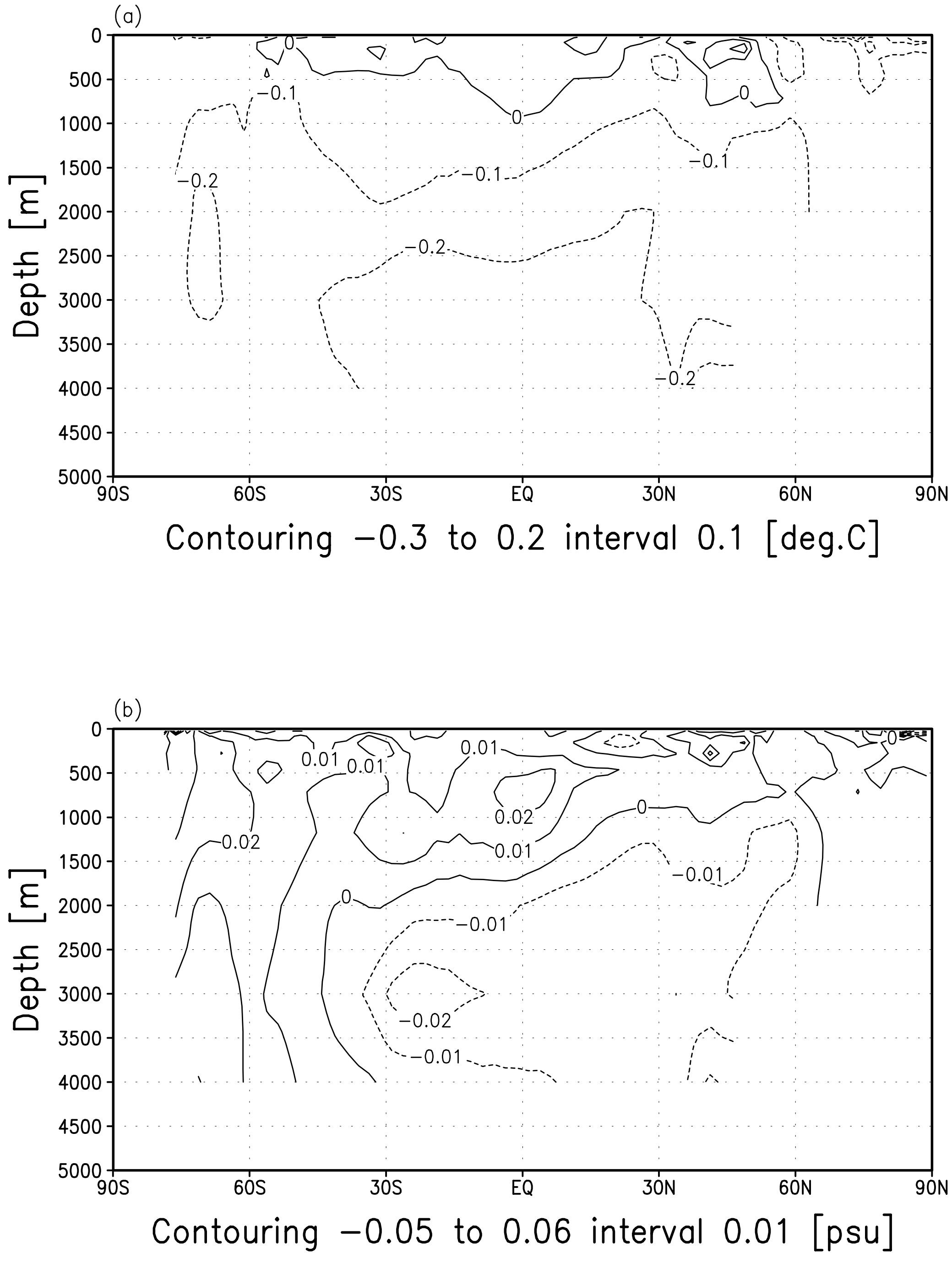

Figure 12. Difference in annual mean convective potential energy release, CCC/V minus CCC.

CCC/L and CCC/CP experiments (L stands for Lead and CP for Coastal Polynya) are performed to identify the role of the enhanced lead fraction. CCC/L reduces the ice concentration by 3 % where and when the ice concentration exceeds 90 % and the air temperature is below the freezing point over the Southern Ocean, and CCC/CP where the grid points are adjacent to Antarctica. The direction of change of the choke point numbers are the same as with CCC/V, while the changes themselves are stronger, in particular with CCC/L. In the Atlantic meridional section of temperature and salinity (Figure 13), CCC/L has much stronger response than with CCC/V, while the pattern of change is remarkably similar to CCC/V. The pattern of CCC/CP minus CCC is similar to CCC/L minus CCC, but the values are about half of that in Figure 13 (not shown). In any case, the difference of temperature and salinity in Southern Ocean is very different from CFC minus CCC (Figure 10). The pattern of Figure 13 indicates enhanced AABW formation by enhanced open-ocean convection. Stronger intrusion of AABW to the north can be explained by cooling and freshening of the deep water north of 30 S. That is similar to CCC/V (Figure 10) but

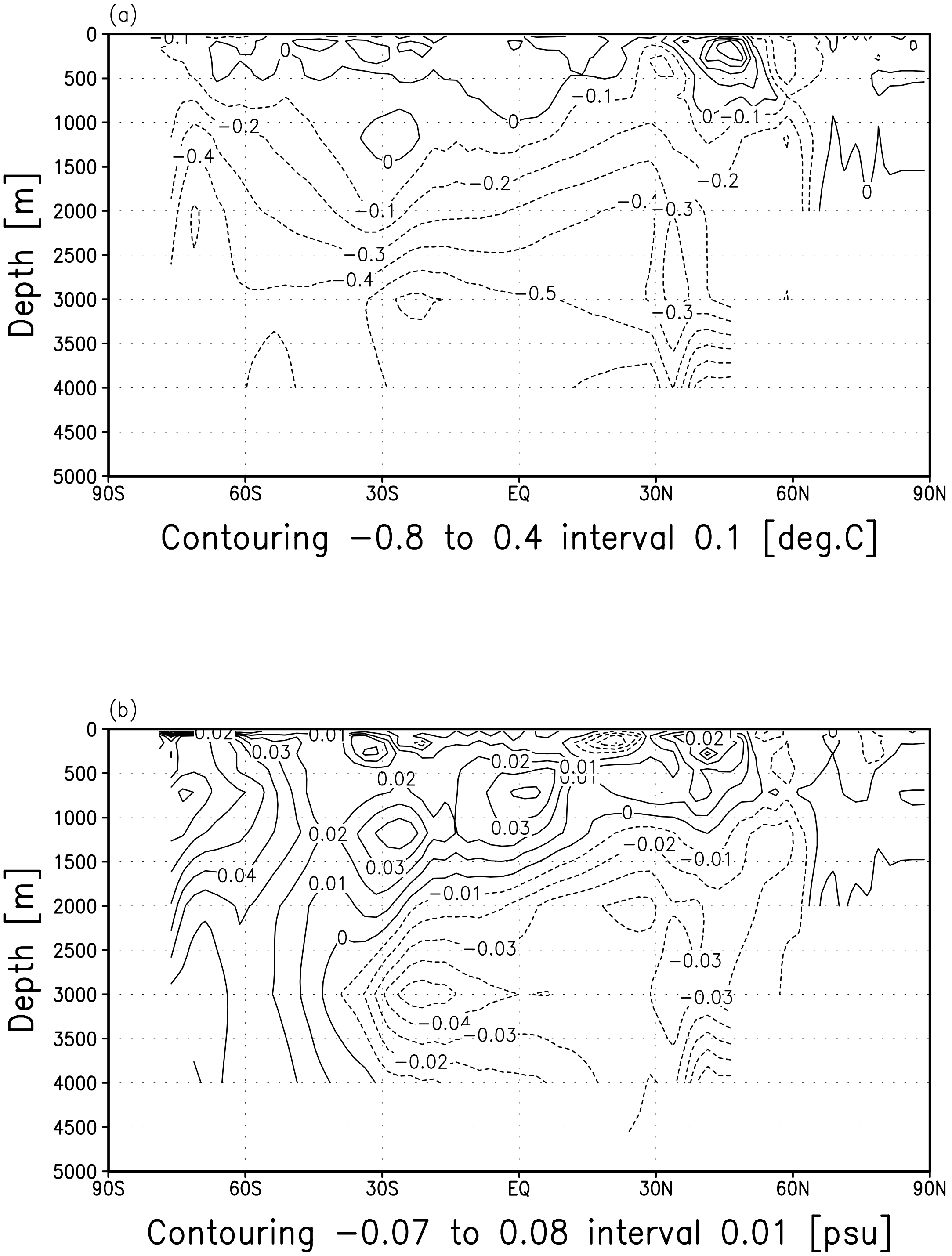

Figure 13. Difference in annual mean convective potential energy release, CCC/L minus CCC.

with much stronger vertical gradients. The latter seems to be associated to a weakening of the AAIW penetration, turning the layers at around 1000 m depth noticeably saltier in CCC/L. The ACC is enhanced in CCC/L and CCC/CP due to the enhanced density gradient across ACC latitude (Figure 13) that results from the colder and saltier conditions south of 60 S.

All three experiments mentioned so far yield substantial cooling in deep ocean same as CFC (versus CCC), but become saltier, as opposed to CFC, which becomes fresher. From the meridional section comparison with CCC, they show reduction of NADW outflow by enhanced AABW formation due to open-ocean convection. The pattern of meridional temperature and salinity change between CFC and the other three experiments also deviating considerably, neither wind variability nor an enhanced lead fraction seems to be able to explain the behavior of CFC. A remaining experiment that might explain the difference between CFC and CCC is the wind treated at the coastal boundary. Arakawa E-grid (Arakawa, 1966) has staggered both vector and scalar points and the boundary falls on the vector points. Thus the wind at the boundary known as katabatic wind that is persistent, very strong and offshore (about 20-30 m/s) is not included in the calculation for ice advection at the offshore vector points. The nearest points for the wind forcing are about 200 km away from the coastline in CCC. The important katabatic wind forcing, the offshore component of which normally turns into an easterly component several tens of kilometers off the coast (Parish and Bromwich, 1991; Goodrick et al., 1998) will thus be lost.

Since CFC has grid points closer to the coastal boundary, the values at the boundary are included in the calculation. Irrespective of how reliable any coastal, katabatic winds of Numerical Weather Prediction (NWP) center analyses actually are (e.g., Broeke et al., 1997; Renfrew et al., 2002), CFC contains additional wind information along the Antarctic coastline. That includes more accurate strong katabatic wind and it pushes sea ice offshore and produces more accurate model representation of coastal polynyas, which are critical for the process of AABW formation. CCC/K (K stands for katabatic wind) is conducted where the scalar point near the coastline is dynamically forced by one (offshore) vector point that includes the adjacent three coastline vector points.

Table 1 and Figure 14 reveal that this modification is indeed crucial for attaining the type of pattern seen in CFC versus CCC. The additional wind information, mostly reflecting offshore (katabatic) winds, works such that it enhances near-boundary convection through enhanced brine release by sea-ice formation in coastal polynyas, while the newly created sea ice seems to provide the appropriate amount of melt water in the open–ocean region (Weddell Sea) to prevent the water column from becoming excessively unstable, thus more realistically maintaining the core properties of CDW south of 60 S. The overall fresher upper layers and the more pronounced AAIW signal in CFC compared to CCC/K is consistent with open-ocean convection being more reduced in CFC versus CCC (Figure 11) than in

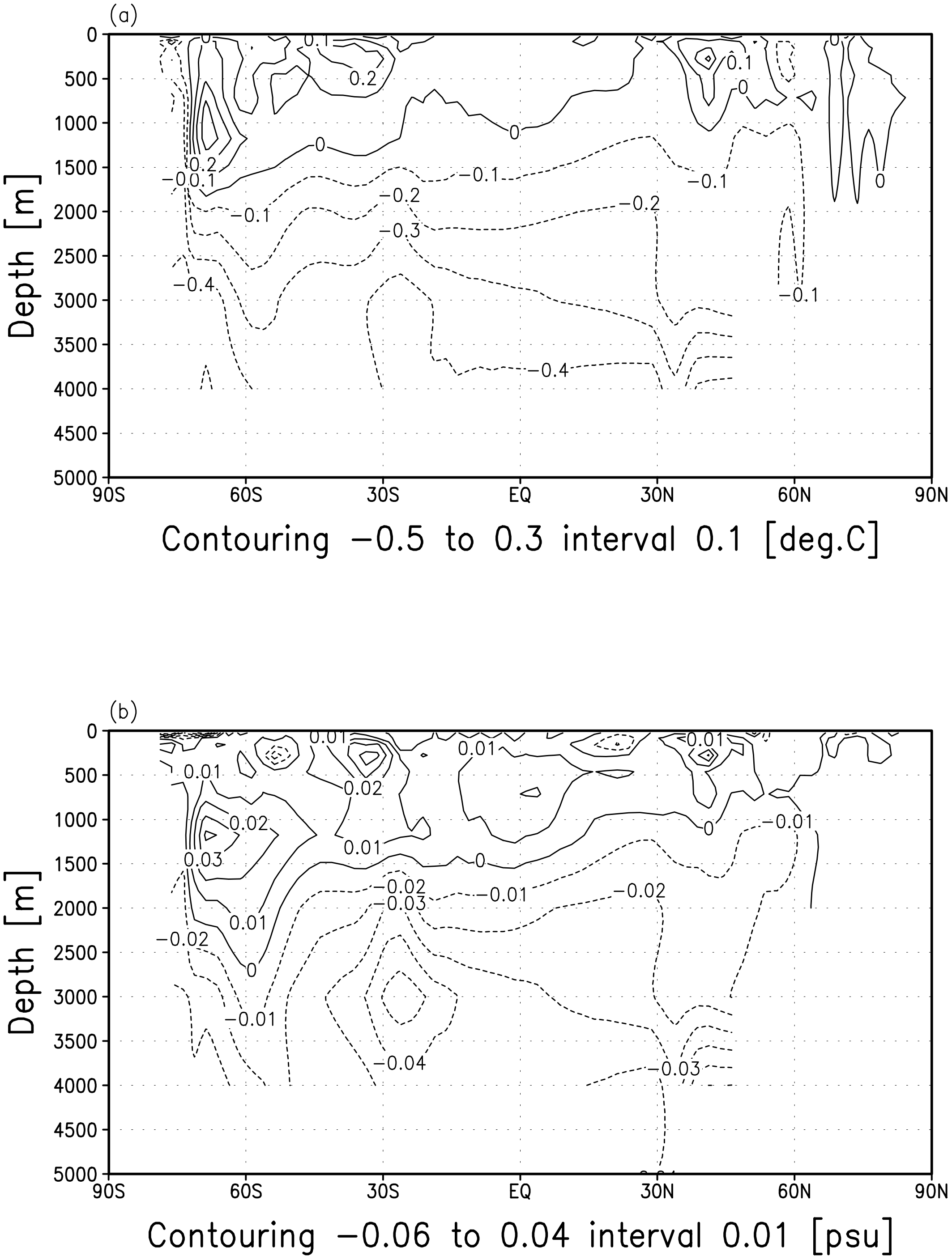

Figure 14. Difference in annual mean convective potential energy release, CCC/K minus CCC.

CCC/K versus CCC (not shown). This also leads to a noticeably reduced ACC in CFC, and a slightly enhanced ACC in CCC/K.

As noted in Section 3.1, the larger discrepancies in CFF cannot be unambiguously related to the refined coastline. The changes versus CCC (and CFC) are nevertheless characterized by the same processes that explain the difference between CFC and CCC, only that they are much stronger in CFF. The difference in convective potential energy release between CFF and CCC reveals a pattern that is similar to Figure 11, but more pronounced (not shown), reflecting a larger reduction of open-ocean convection. The substantial cooling and freshening of the deep ocean is a result of enhanced AABW formation through enhanced near-boundary convection. In this simulation, the locations of the associated source-water mass formation sites should have the closest possible geographic correspondence to the real world under the given resolution.

3.3 Conclusions

In this chapter it was demonstrated that enhancing the resolution of the sea-ice component of a global coarse-resolution ocean GCM is a viable option for improving the critical high-latitude surface buoyancy forcing while retaining the necessary efficiency of the model to investigate the long-term global deep-ocean response. The presented 9-fold resolution enhancement constitutes an intermediate step toward an 81-fold enhancement (see Chapter IV), at which point the pixel resolution of satellite passive microwave data that is routinely used to retrieve sea-ice concentration (Gloersen et al., 1992; Markus and Cavalieri, 2000) is reached. The ultimate goal is to verify the simulated sea-ice concentration on the same space and time scale as available from satellite-derived data, which is a step toward systematically identifying problems in coupled atmosphere - sea-ice - ocean GCMs.

The higher-resolution sea-ice component reveals a more detailed sea-ice texture, associated, in particular, with a more detailed representation of coastal polynyas and a sharper ice edge, both of which are in better agreement with observations. The higher resolution results also in a more realistic ice-thickness distribution in the Weddell Sea, which encompasses multi-year ice. Compression and polynya formation along the coarse coastline are physically realistic. The coastline has been adjusted to the finer grid in an additional model version, where coastal grid points have been partially covered by pseudo fast ice following the sea-ice/ocean - ice-shelf/land demarcation line of the satellite-microwave data. This measure ensures the closest possible geographical matching of coastal polynya occurrence.

The long-term global deep-ocean impact of enhancing the resolution of Southern Ocean sea ice is relatively small, but noticeable. While a major impact of this measure is an overall reduced sea-ice concentration, an according enhancement of the wind variability or an according reduction of ice concentration led to a global response pattern that is different from that associated with the higher sea-ice resolution. In particular, the pattern of the former two was more representative of one that is associated with enhanced AABW formation through enhanced open-ocean convection, as opposed to the one seen with the higher-resolution sea-ice component, which indicated less open-ocean convection, and more near-boundary convection instead. The decisive reason for this behaviour turned out to be the incorporation of the coastal winds in the higher resolution model version, which were idle in the coarse resolution version. This result demonstrates that a detailed description of the coastal (in particular katabatic) winds along Antarctica plays a vital role in determining long-term global deep-ocean properties and circulation through their direct impact on brine release due to freezing in coastal polynyas and its ultimate impact on the formation of AABW. It also showed that the formation of AAIW is getting affected by the resolution of the sea-ice component.

CHAPTER IV

81-FOLD HIGHER-RESOLUTION SEA ICE IN LONG-TERM GLOBAL OCEAN GCM INTEGRATIONS[•]

Building on the approach taken for the research described in the previous chapter, the sea-ice component is enhanced by another factor 9 such that each coarse ocean grid cell south of 50 S is coupled to 81 sea-ice grid points where sea ice emerges. This brings the resolution of the sea-ice component close to 22 km, and thus within the pixel resolution of the SMMR and the SSM/I data, and allows for a rigorous verification of the simulated sea ice while the global ocean GCM is still efficient enough for equilibrium integrations on the order of 1000 years to be undertaken. The matching of the space and time scales between Southern Ocean sea-ice model and satellite-derived product allows also for a detailed verification of the high-

---

[•] A few passages in this chapter have been published in "High-Resolution Sea Ice in Long-Term Global Ocean GCM Integrations" by Achim Stössel, Marion Stössel and Joong-Tae Kim, 2007. Ocean Modelling, 16, 206-223, and are reproduced here with permission by Elsevier 2007.

frequency variability along the ice edge and the coastal polynyas, the representation of the latter being most crucial for a half-way realistic simulation of AABW formation (e.g., Gordon, 1998; Orsi et al., 2002; Whitworth et al., 1998).

4.1 Experiments and Results

4.1.1 Evaluation of Sea-Ice Concentration

The experiments discussed in this section are summarized in Table 2. They constitute a hierarchy of experiments in which modifications have been added to successively improve the modeled sea-ice concentration as verified against the corresponding satellite-derived product. As in Chapter III this product relies on the "NASA Team 2" (NT2) algorithm (Markus and Cavalieri, 2000). NT2 is a recent refinement to earlier algorithms that convert satellite remote-sensed passive-microwave signals to sea-ice concentration. For the application of this algorithm to verify simulated Antarctic coastal

Table 1. The hierarchy of model experiments I-V. SEA ICE: Southern Ocean sea ice 81-fold higher resolution than ocean model. CONVECTION: convection parameterization in Southern Ocean resolved on same grid as sea ice. TEMPERATURE: temperature of upper-ocean layer modified to be a function of high-resolution ice concentration. PLUME: plume velocity reduced from 0.03 m/s to 0.004 m/s. TIDES: pseudo tidal variability introduced to modify Southern Ocean sea-ice pack.

Experiments	SEA ICE	CONVECTION	TEMPERATURE	PLUME	TIDES
I	X				
II	X	X			
III	X	X	X		
IV	X	X	X	X	
V	X	X	X	X	X

polynyas, and for its comparison to the "Bootstrap" algorithm (Comiso et al., 1997) in this regard, see Stössel and Markus (2004).

Figure 15-I shows the mid-September snapshot of ice concentration as simulated in experiment I. Comparing to the satellite-derived data (Figure 15-NT2), high-resolution sea-ice model embedded with coarse-resolution ocean GCM does not look very similar to nature. Within the ice pack, polynyas of the size of coarse grid emerge sporadically in space and time. Polynyas are mainly related to the surface temperature and convection. The ice edge shows coarse-grid pattern which is expected wherever the upper-ocean temperature plays a large role in determining sea ice. Concerning the apparently spurious coarse-grid pattern, it should be noted that a smooth ice edge or smooth isolines of any model variables are of course an artifact of interpolation: a model grid cell contains just one value per variable, which should make isolines actually always follow the structure of a model's grid. In this and the following illustrations the isolines are drawn for the fine-grid variables, thus, coarse-grid

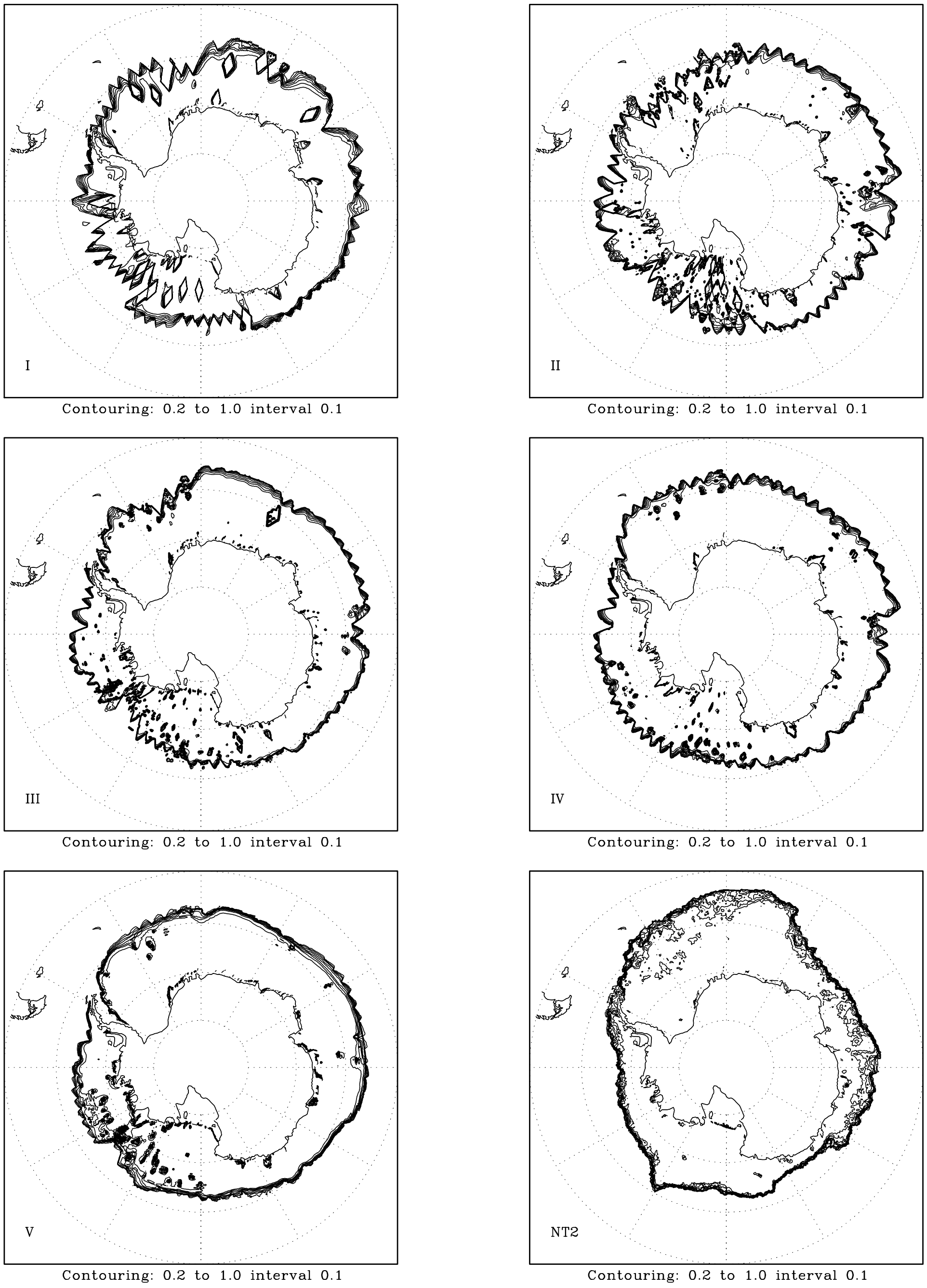

Figure 15: Mid-September snapshots of ice concentration (1 = 100 %) as simulated in experiments I-V and as derived from satellite passive microwave data using the NT2 algorithm.

patterns, if any, will readily emerge. The winter seasonal mean ice concentration (Figure 15-I) shows a more pronounced coarse-grid pattern.

The coarse-grid pattern polynyas decrease when the one-dimensional convection parameterization is reduced to the size of sea-ice grid. An improvement is noticeable when anomalies of potential temperature (θ) and salinity (S) at each layer are preserved during the time integration of the model. These θ and S ‘anomalies’ are defined as fine-scale departures from the coarse-grid mean at the end of each time step. Thus, each fine grid variable can hold different preconditioning for convection. In this experiment (Figure 15-II), the polynyas due to oceanic heat flux associated with convection are more widespread, approaching the scale of the fine grid.

Experiment III is based on the assumption that the water surrounding sea ice is always at or very near its freezing point. The thickness of the upper layer of an ocean model is typically on the order of 10 m (in this model actually 50 m). If warmer than the freezing point temperature, this excess energy is normally used to instantaneously melt any ice in the grid box until the freezing point is reached or the ice is gone, such that energy is conserved. To reduce this effect, the upper-layer has been modified is a function of ice concentration by

$$T_1^{new} = 0.5T_1^{old} + 0.5\left[N_i T_f + (1-N_i)T_1^{old}\right],$$

where, N_i is ice concentration, T_1 is the temperature of the ocean model's upper layer and T_f is the freezing point temperature. This effect cools the upper layer when sea ice is present. Figure 15-III shows this result, which reduces the coarse-grid pattern and polynyas, and increases the sea-ice extent and thickness as expected.

When Figure 15-III is compared to the satellite-derived data (Figure 15-NT2), it shows more polynyas within the winter ice pack in the Pacific Ocean sector. The plume convection parameterization contains many empirical parameters such as the initial plume radius, initial plume velocity, and the fractional area of plume (Paluszkiewicz and

Romea, 1997), so it is tempting to investigate the sensitivity of any of these parameters. Initial plume velocity is the most sensitive parameter. In experiment IV (Figure 15-IV), the initial plume velocity is changed from 0.03 m/s to 0.01 m/s. This is a heuristic experiment; for more systematic investigations on the effect of various convection parameterizations, and discussions on their ability to capture the real-world physics see e.g. Marshall and Schott (1999), Timmermann and Beckmann (2004) and Canuto et al. (2004). Figure 15-IV reduces number of open-ocean polynyas, and a reduced number and extent of coastal polynyas, all more commensurate to the satellite-derived data. The ice extent in the Indian Ocean section and the Pacific Ocean section is generally too large.

Experiments I-IV have very static ice edge comparing to the wave-like variability in satellite-derived data in spite of using atmospheric synoptic wind variability. When comparing fortnightly or monthly means (Figure 16) with daily snapshot (Figure 15), the variability is more apparent. Experiments I-III show some variability associated

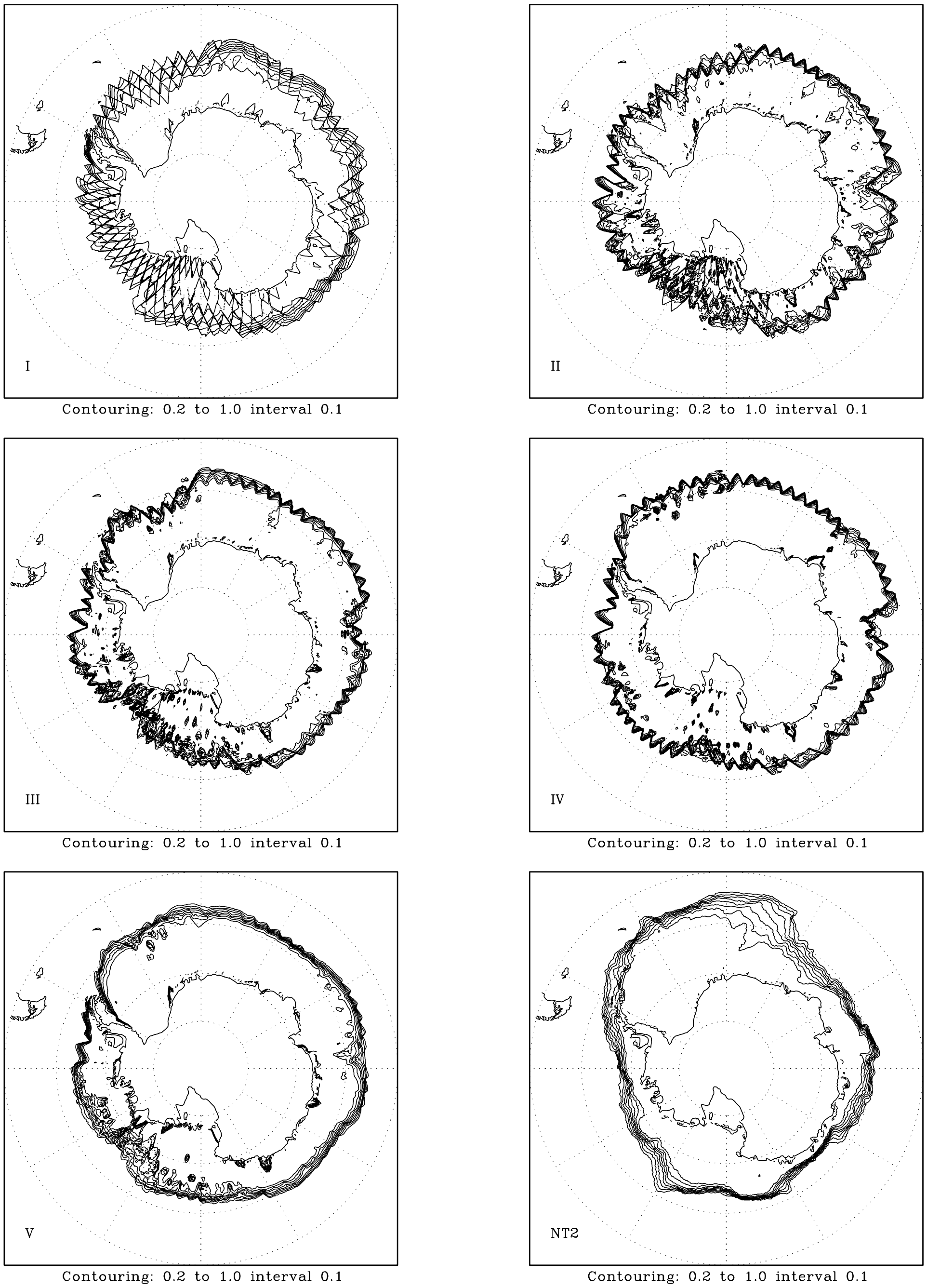

Figure 16: Mid-September means of ice concentration (1 = 100 %) as simulated in experiments I-V and as derived from satellite passive microwave data using the NT2 algorithm.

with convection, Experiment IV shows hardly any variability even along the ice edge not only snapshot but also winter mean. The satellite-derived ice concentration shows wide variability along the ice edge on both snapshot and winter mean. In recent literature, considerable discussion has emerged on the importance of tidal currents for a realistic representation of Southern Ocean sea ice (e.g., Heil and Hibler, 2002; Eisen and Kottmeier, 2000; Koentopp et al., 2005; Padman and Kottmeier, 2000). The primary effect of high-frequency variability on sea ice is an overall enhanced lead fraction, which itself would yield more new-ice formation and thus dense water formation in winter time, likely contributing to an enhanced production AABW. In experiment V, high-frequency variability of upper-ocean currents has been introduced to just influence the high-resolution Southern Ocean sea-ice pack. This pseudo tidal variability features a complete cycle (period) within the 20 hour time step of the coarse model, and is projected onto the 5 hour time stepping of the high-resolution ice dynamics by assuming the water underneath the ice to first move with 0.3 m/s due north-eastward, followed by a cease (slack), then to move with the initial speed in the opposite direction, to be followed again by a slack. This is clearly a very crude way of introducing tidal or inertial variability, but at least gives some hint on what such type of variability could mean for Southern Ocean sea ice.

Comparing Figure 15-V with Figure 15-IV, the ice edge appears wider with a reduced coarse-grid pattern, and in much better agreement with the satellite-derived data (Figure 15 and Figure 16, Experiment V versus NT2). The coastal polynyas generally extend within the observed range, though they tend to be overestimated. The coastal polynyas along the boundary are closer to the satellite-derived passive-microwave data using the "bootstrap" algorithm (Comiso et al., 1997; Stössel and Markus, 2004).

The variation of ice concentration along the ice edge of Experiment IV and V as well as NT2 are shown in Figure 17. The latter shows a broad band connecting along the ice edge, indicating a spatially

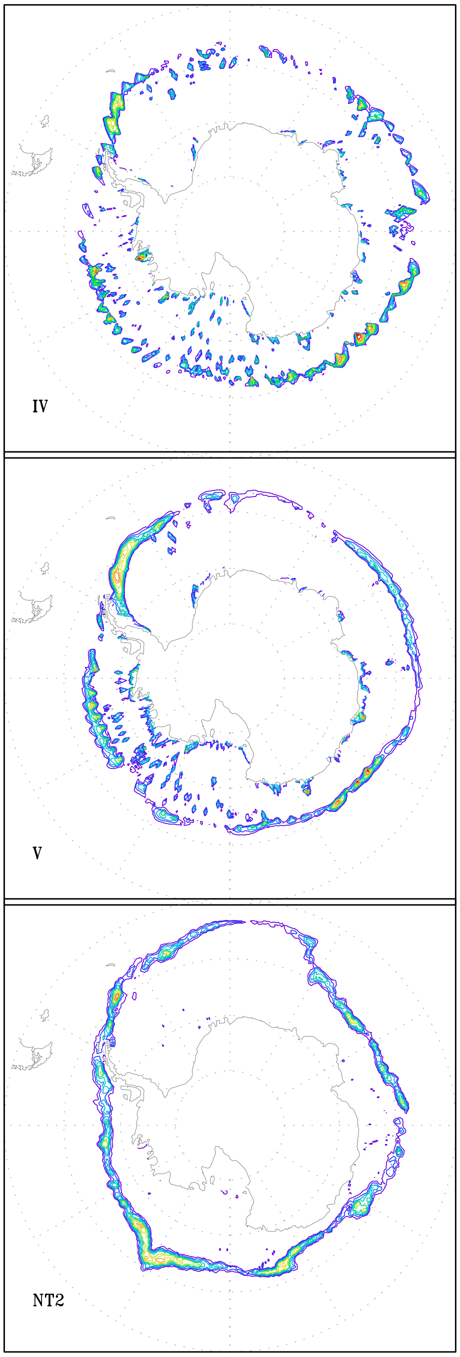

Contouring: 0.02 to 0.2 interval 0.02

Figure 17: September variance of ice concentration, as simulated in experiment IV (upper panel), experiment V (middle panel), and as derived from satellite (bottom panel).

correlated, wave-like pattern (Figure 17-NT2). Experiment V (Figure 17-V) shows similar pattern to NT2 but much weaker and not at the same locations as derived from satellite. In Figure 17-IV, Experiment IV shows the variability is disconnected and not correlated. It mainly reflects local variability due to small-scale convection along the ice edge. Note also the difference in coastal polynya occurrence. With NT2, there is no noticeable variability, as opposed to Experiments IV and V.

Another means of looking at the high frequency as well as the seasonal variability is a time series of ice concentration along a meridional section, as in Figure 18 along 30 W. To demonstrate the highly beneficial effect of considering high-frequency (similar to tidal) variability of ocean currents, experiment IV has been added for comparison. While discrepancies such as a larger abundance of coastal polynyas and a more rapid decay in the spring are noticeable when comparing experiment V with NT2, there is overall a very good

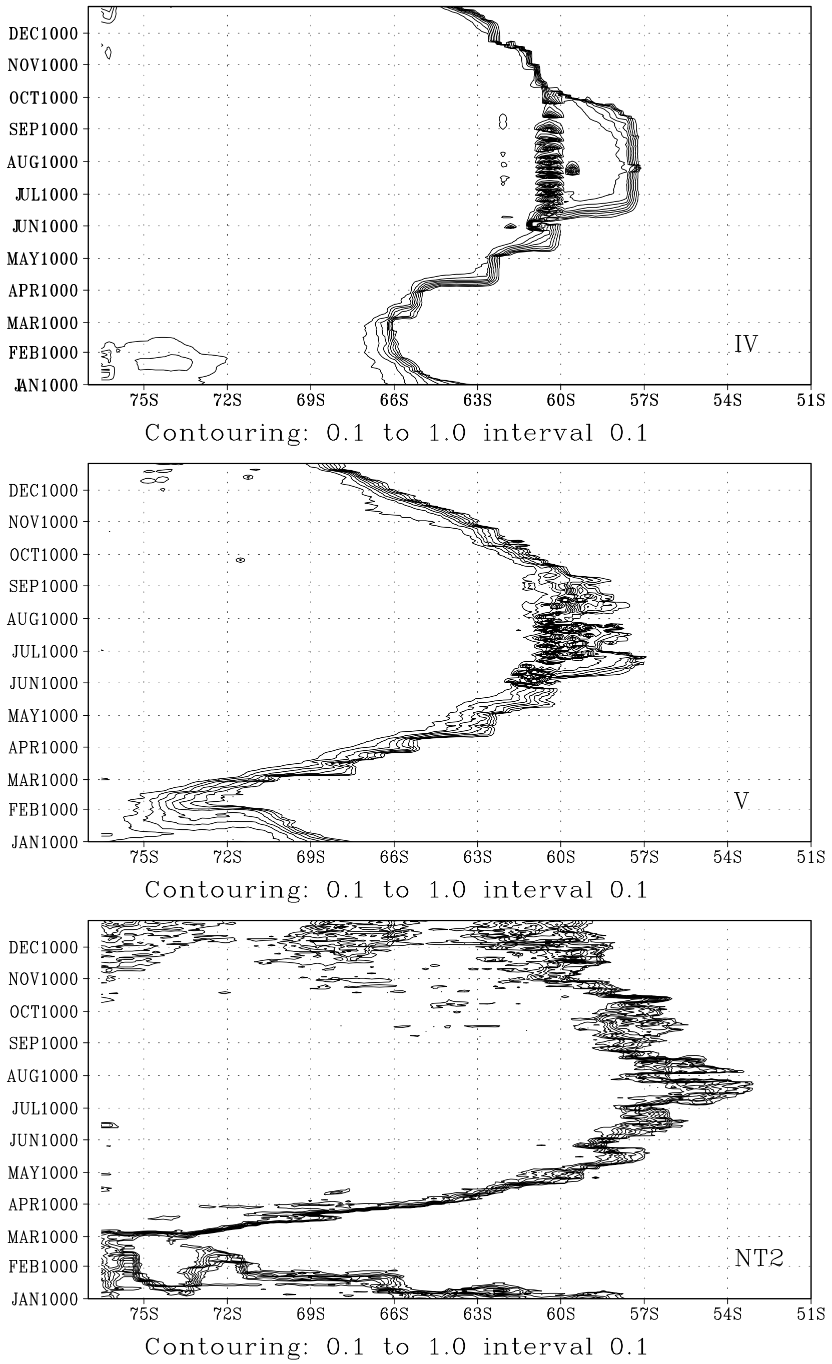

Figure 18: Seasonal evolution of ice concentration along 30 W, as simulated in experiment IV (upper panel), experiment V (middle panel), and as derived from satellite (bottom panel).

agreement, as opposed to experiment IV, which lacks any of the observed variability.

Figure 19 shows the seasonal change in ice area for the entire Southern Ocean sea-ice pack, with the full thick line representing the NT2 product. The first striking discrepancy to notice with all experiments is the too rapid increase in ice cover in fall, a situation also encountered in earlier modeling studies with global ocean GCMs (e.g., Timmermann et al., 2005; Kim and Stössel, 2001). Another severe discrepancy is the overestimation of winter ice area, in particular in the experiments where there is a direct sea-ice feedback on the upper-ocean temperature (experiments III-V). A distinct feature of the observed Antarctic sea-ice seasonality is its asymmetry, characterized by a slow extension and a fast retreat. This is in particular not captured in experiments IV and V, where the plume velocity has been reduced. This is consistent with the findings of Kim and Stössel (2001): the penetration of convection being described to occur on a smaller scale with the plume convection

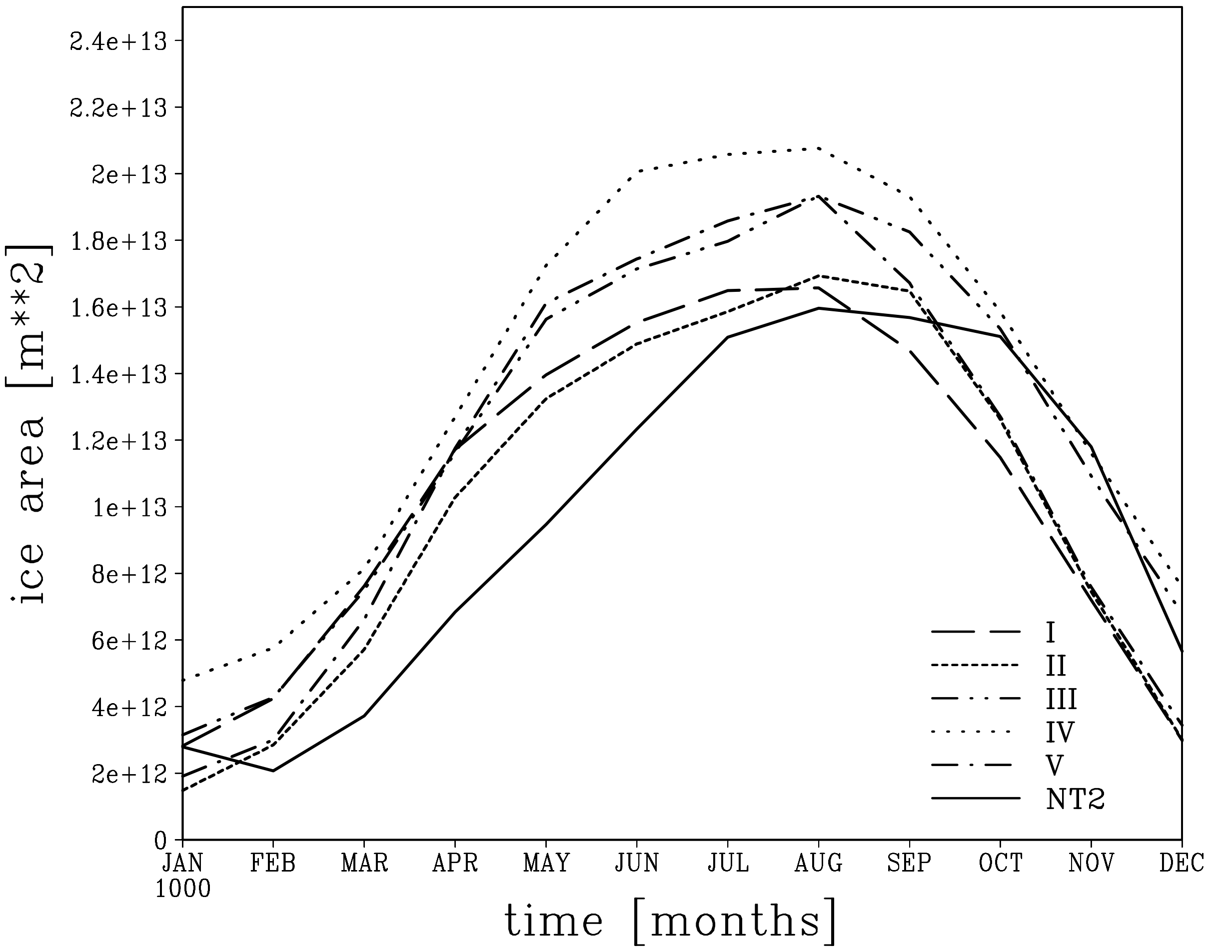

Figure 19: Seasonal cycles of ice area as simulated experiments I-V (as marked), and as derived from satellite (thick solid line).

parameterization than with conventional convective adjustment contributes to the observed asymmetry of the seasonal cycle by allowing the warm Lower Circumpolar Deep Water (LCDW) to be tapped during the ice growth season. Reducing the plume velocity diminishes this effect, thus leading to a more symmetric seasonal cycle. Otherwise it is worth noting that the high-frequency variability of upper ocean currents leads to a lower (more realistic) summer ice area than without (experiments V versus IV), but also to a too rapid ice retreat, peaking in winter about two months earlier than observed.

A closer look is taken at the September-mean ice-thickness distribution in the Weddell Sea (Figure 20-a), as well as at its satellite-derived ice-concentration counterpart based on NT2 (Figure 20-b). In terms of ice-thickness observations, this region is characterized by the thickest ice (2-4 m) occurring in its western part (e.g., Strass and Fahrbach, 1998; Harms et al, 2001). Such is clearly not simulated in experiment V, and even less so in any of the

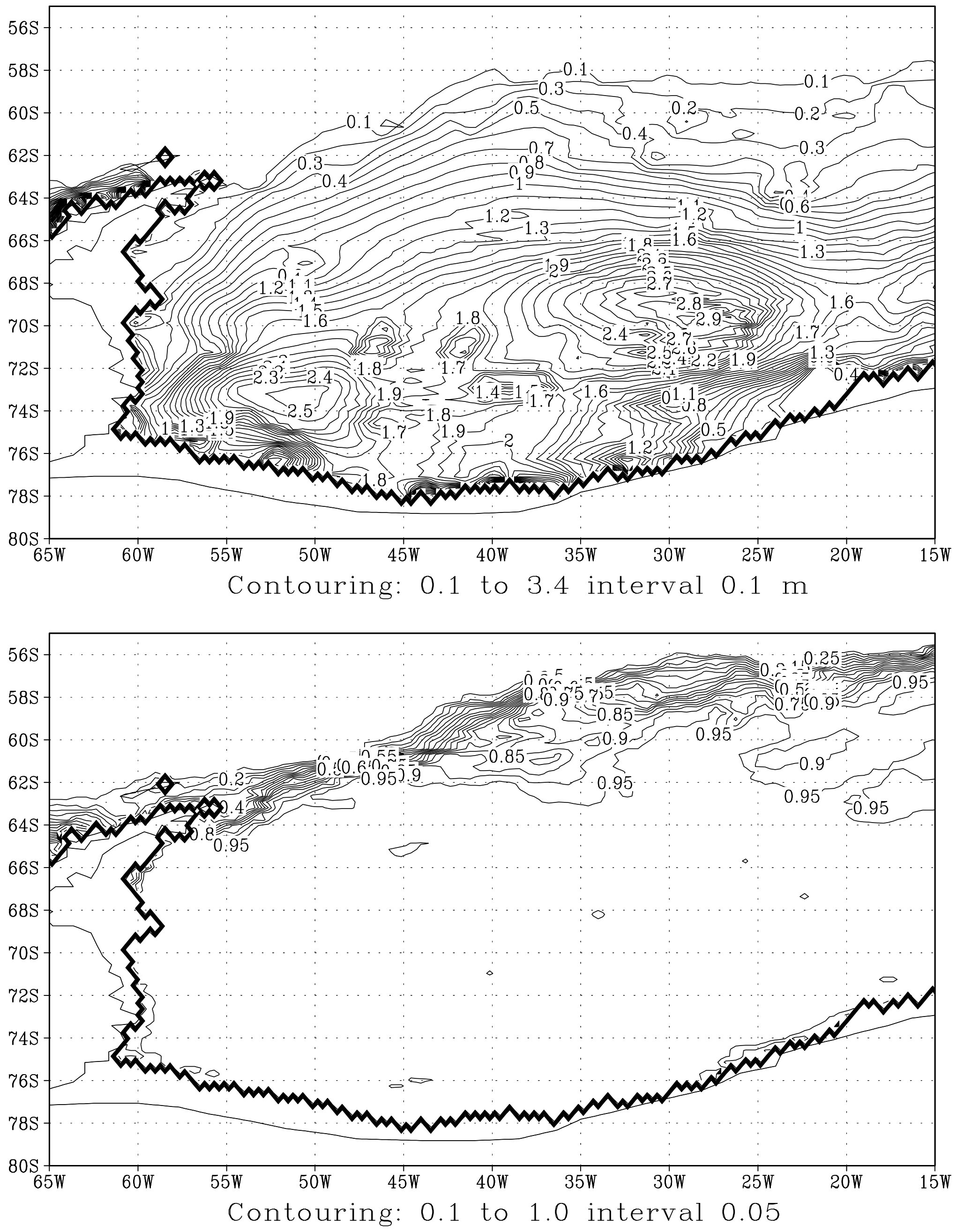

Figure 20: September-mean ice thickness as simulated in experiment V (upper panel) and September-mean ice concentration as derived from satellite (lower panel), for the western Weddell Sea.

other experiments. To what extent the character of the simulated spatial inhomogeneities in ice thickness are realistic is hard to verify. Based on measurements with upward looking sonars (Strass and Fahrbach, 1998), the thicknesses around 70 S and 25 W seem to be reasonable, while they are severely underestimated within 10° longitude east of the Antarctic Peninsular. A similar deficiency has been noted in Timmermann et al. (2005).

4.1.2 The Long-Term Oceanic Response

The strategy of the experiments described in this chapter is to refine the simulation of Southern Ocean sea ice in a framework that is coupled to a global ocean GCM, and in equilibrium with its circulation and global water-mass distribution. This is a higher challenge than running a regional sea-ice - ocean GCM or a global sea-ice - ocean GCM for a few decades, since the long-term thermohaline circulation may eventually change to a point where Southern Ocean sea ice cannot be maintained at its currently observed characteristics. Changes in the convection parameterization to improve Southern Ocean sea ice may e.g. lead to a substantial reduction of AABW formation, which will (after several hundred years of model integration) lead to a stronger outflow of North Atlantic Deep Water (NADW), and eventually to warmer and saltier LCDW. In such a scenario, any convection in the Southern Ocean will lead to much warmer water penetrating to the surface, with a corresponding negative impact on the ice cover. So the issue here is to simultaneously investigate the long-term global ocean properties, and see how their equilibrium response differs with experiment and from the observed climatology.

Table 3 summarizes some key integrated variables. A rather straightforward relationship is that between the Atlantic meridional heat transport across 30 N, the NADW outflow across 30 S, and the Arctic ice volume. I.e., with enhanced NADW outflow there is a larger North Atlantic overturning, a larger northward heat transport, and thus a reduced Arctic ice volume. Among our experiments, there is

Table 2. Annual equilibrium values of selected integrated or averaged variables as simulated in experiment I-V. HEAT: Atlantic northward heat transport across 30 N [PW]. NADW: NADW outflow across 30 S [Sv]. ACC: Drake Passage throughflow [Sv]. HARC: Arctic sea-ice volume [10^{12} m^3]. HANT: Antarctic sea-ice volume [10^{12} m^3]. θ_4: global-mean potential temperature at 4000 m depth [^{o}C]. S_4: global-mean salinity at 4000 m depth [psu]. FR^2: Southern Ocean net freezing rate squared [m^2]. CONV: convective potential energy release averaged south of 50 S [W/m^2].

Experiments	HEAT	NADW	ACC	HARC	HANT	θ_4	S_4	FR^2	CONV
I	0.62	12.2	95	17.7	11.9	1.06	34.672	0.64	2.61
II	0.64	19.2	95	17.2	7.1	2.10	34.721	0.17	1.92
III	0.62	17.4	98	17.4	10.7	1.84	34.718	0.20	2.21
IV	0.69	20.3	100	17.0	11.6	2.91	34.816	0.33	0.65
V	0.66	18.2	109	17.1	9.5	2.68	34.816	0.80	0.81

also a direct relationship between the outflow of NADW, the formation of AABW and its intrusion into the Atlantic, and the global deep-ocean properties. In particular, reduced AABW intrusion leads to an enhanced outflow of NADW, and thus warmer and saltier global deep-ocean properties.

The relationship of all this to the strength of the ACC as well as to the Southern Ocean ice volume is less obvious. To explain this relationship, two other variables are added, namely the square of the net freezing rate to indicate the amount of annual freezing and melting, and the annual convective potential energy release (in W/m^2), both averaged over the entire Southern Ocean. Colder and fresher global deep-ocean properties are thus clearly correlated with enhanced convective potential energy release in the Southern Ocean, which leads to enhanced AABW formation. The annual freezing-melting cycle, on the other hand, is not correlated with the amount of convection, but rather with the strength of the ACC, except when convection is high. I.e., when the freezing-melting cycle is high, and convection is low, as in experiment V, a stronger meridional density gradient establishes, and thus a stronger ACC. If a high freezing-melting cycle coincides with a high convection rate, however, a strong meridional density gradient does not build up.

This relationship becomes more apparent when looking at meridional temperature and salinity sections of all five experiments. Figures 21 and 22 show such for February, as averages between 50 W and 30 W, i.e. along a sector of the Weddell Sea, in addition to the corresponding sector of the Levitus (1982) climatology. A summer month has been chosen because oceanographic observations in the Weddell Sea are almost exclusively taken during the summer season when ships are less hindered by sea ice (Orsi, pers. comm., 2005). Experiment I sticks out by an almost homogeneous water column between 200 and 1000 m south of 60 S, commensurate with a strong convection rate, as found from Table 3. As a result, there is a strong meridional density gradient in this layer between 65 S and 55 S, i.e. the latitudes of the Drake Passage. In the other extreme, where there

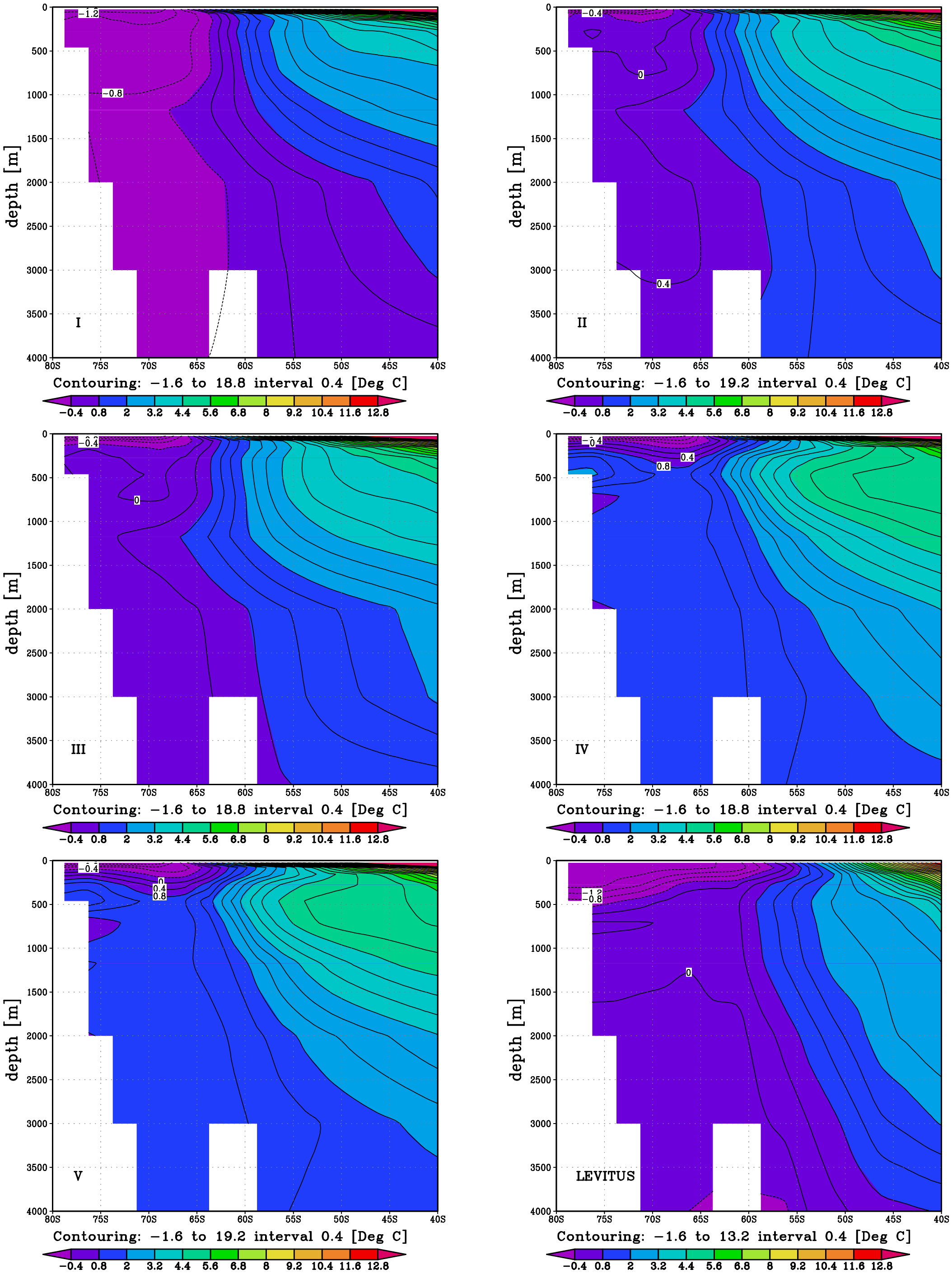

Figure 21: February potential temperature sections as simulated in experiments I-V, and as derived from measurements based on the Levitus climatology; all sections are average between 50 W and 30 W.

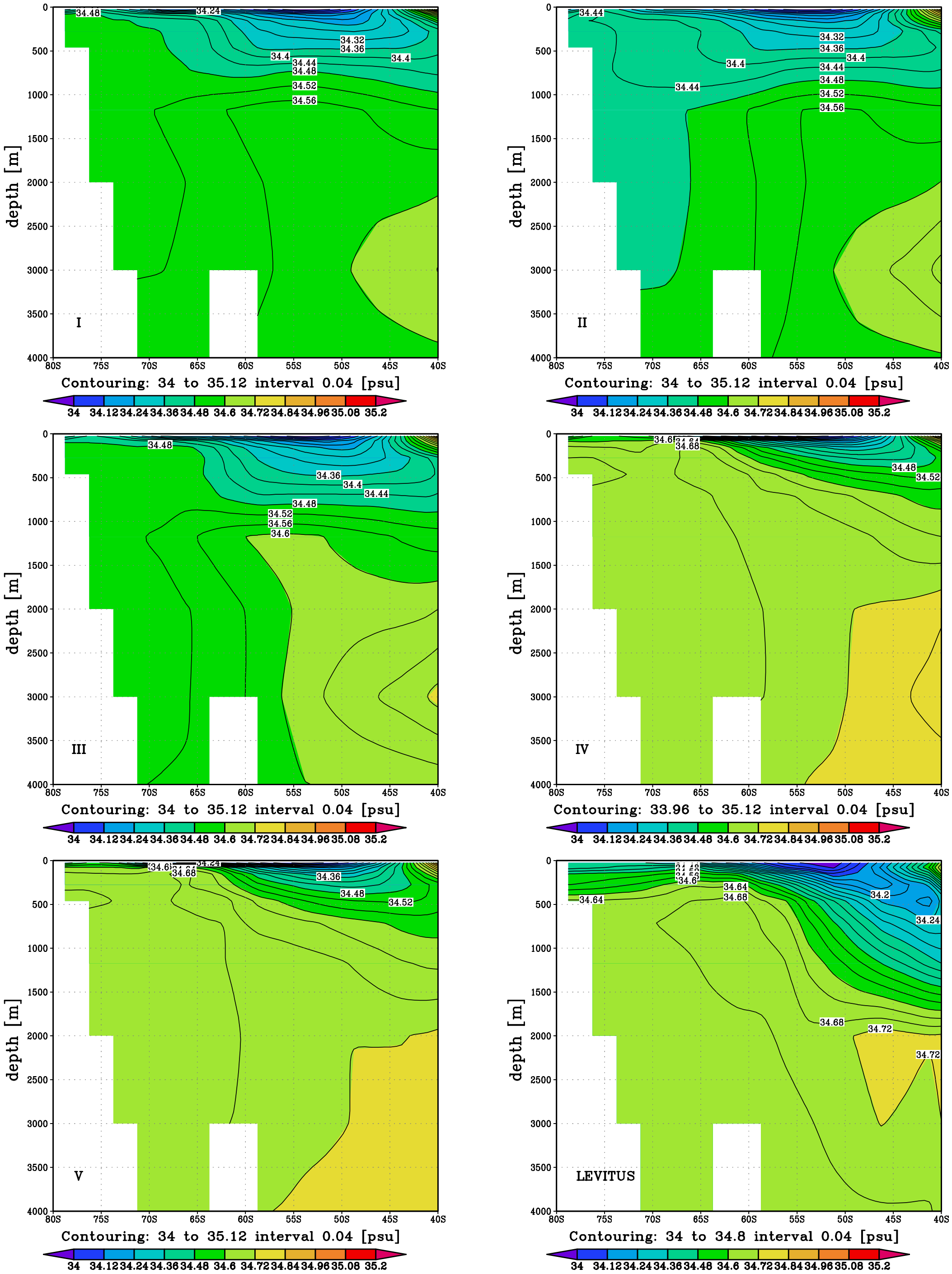

Figure 22: February salinity sections as simulated in experiments I-V, and as derived from measurements based on the Levitus climatology; all sections are average between 50 W and 30 W.

is a strong freezing-melting cycle, a strong ACC, but a weak convection rate, the warm and salty LCDW tongue is very pronounced, the pattern being not too dissimilar from the Levitus climatology, though too warm. The reduction in convection as imposed in experiments IV and V is thus very effective in maintaining a strong enough stratification in the Southern Ocean for a pronounced LCDW pattern to emerge, and this pattern is becoming amplified when some sort of tidal variability is considered to influence the ice pack. This more realistic LCDW pattern naturally leads to a more realistic meridional density gradient across the Drake Passage latitudes, and thus a more realistic ACC, the observed figure lying around 130 Sv (Whitworth and Peterson, 1985; Cunningham et al., 2003).

While there are obvious deficiencies in the temperature and salinity sections of all experiments when compared to the observed climatology, there is still a striking improvement toward the distinct observed pattern of LCDW when the upper-layer temperature and/or the plume velocity are manipulated (experiments III-V). While the temperature at 500 m depth in experiment V is overestimated by 1 to 2 K, the sharp vertical change south of 65 S in the upper 300 m is more than what is found from the Levitus climatology, and closer to what individual WOCE sections show (e.g., Orsi and Whitworth, 2004). On the other hand, the AAIW signal is far too weak, and the cold AABW is missing. Furthermore, the global deep-ocean properties are too warm and salty (the Levitus climatology values reading 1.08°C and 34.73 psu, respectively), commensurate with a too strong outflow of NADW across 30 S. Thus, even though the Southern Ocean stratification and a series of sea-ice characteristics were improved through the hierarchy of model experiments, the global deep-ocean properties and circulation do not approach an equilibrium that is in reasonable agreement with present-day observed conditions.

4.2 Conclusions

The resolution of the sea-ice component of a global ocean GCM has been increased to about 22 km, i.e. to about the pixel resolution of satellite passive microwave data from which sea-ice concentration is routinely derived. The resolution of the ocean component is an order of magnitude coarser to allow for investigations of the long-term response of the thermohaline circulation to changes in the model's high latitudes, and how such response feeds back onto the high-latitude conditions. While both polar regions are included, the focus in this study was the southern hemisphere high latitudes, to which the embedding of the high-resolution sea-ice component has been restricted.

The approach taken allows for a thorough verification of sea ice, a model variable that is critical in determining the high-latitude conditions of a global ocean model. At the same time, sea ice is highly sensitive to changes of its ambient conditions, especially winds and oceanic heat flux. The latter is in the Southern Ocean mostly determined by warm LCDW penetrating to the surface via convection. Convection, on the other hand, is a subgrid-scale process that is typically not resolved by the governing equations of a global ocean GCM. Its parameterization is difficult due to its associated processes being highly nonlinear, and is still a major challenge in global ocean modeling (e.g., Canuto et al., 2004). Thus, no matter how sophisticated a sea-ice model or how detailed its atmospheric forcing, in the Southern Ocean its performance will depend critically on the parameterization of oceanic convection. In combination with the surface buoyancy fluxes, which themselves are critically dependent on the sea-ice conditions, complex nonlinear interactions emerge, the integrated effects of which eventually determine the rate of AABW formation. Any changes of that rate lead to long-term changes of the global thermohaline circulation, which will ultimately be reflected in changes of the properties of LCDW. These could again influence the Southern Ocean ice cover, thus closing a long-term feedback loop.

In a series of experiments, the current approach of embedding a high-resolution sea-ice component into a coarse ocean GCM has shown to be robust. Without refining the one-dimensional convection parameterization, coarse-grid patterns emerge due to the strong dependence of sea ice on the ocean model's upper-layer temperature. Further improvements toward some of the satellite-derived sea-ice characteristics were accomplished by manipulations of the empirical parameters of the convection parameterization and/or the upper-layer temperature. These measures, however, did not improve the total ice area and extent, which are substantially overestimated during the fall and winter seasons, and mostly underestimated during the spring season, resulting in a too symmetric seasonal cycle. The observed asymmetry having been related to the beneficial property of plume convection by enabling LCDW to penetrate to the surface in the fall season to retard ice growth and expansion suggests that the threshold for deep-penetrating convection may have to be adjusted to more closely follow the ice growth rate.

Vertical-meridional sections of temperature and salinity in the Southern Ocean indicate that the distinct LCDW pattern can be reproduced when convection is reduced and the upper-ocean temperature more constrained by the simulated ice conditions. Reduced (open-ocean) convection underestimating the rate of AABW formation, however, leads to a long-term overestimation of the global mean deep-ocean temperature and salinity, i.e. a stronger than currently observed global influence of NADW. This may hint toward AABW formation via near-boundary convection being underestimated in these model settings.

For an additional set of experiments and discussions on this subject, see Stössel et al. (2007).

CHAPTER V

CONCLUSIONS

The general purpose of this study is to bridge the gap between regional high-resolution high-latitude models and global models used for climate studies in which critical high-latitude processes are represented at coarse resolution. The large-scale deep-ocean water masses are to a large extent formed by high-latitude convection and physical processes on the horizontal scale of the order of 1 km. In Chapter III, the higher-resolved sea-ice component restricted to the Southern Ocean yields more detailed structures, such as a more detailed representation of coastal polynyas, a realistically sharp ice edge, and an overall enhanced lead fraction. The latter gives rise to a somewhat enhanced rate of Antarctic Bottom Water formation through enhanced near-boundary convection, which is reflected in slightly cooler and fresher global deep-ocean properties and a reduced Antarctic Circumpolar Current as a result of reduced open-ocean convection. In a set of sensitivity experiments, the difference pattern between the higher- and the coarse-resolution sea-ice component versions has been identified to be due to local details of the katabatic wind fields along the Antarctic coastal boundary.

In Chapter IV, the results suggest that the long-term global deep-ocean properties and circulation are highly influenced by the model resolution of the Antarctic coastal boundary. Synoptic-scale wind variability does not seem to be sufficient to explain the observed variability along ice edge, and the lead fraction; the results suggest that adding variability due to tidal currents is potentially able to reduce this deficiency. The amount of vertical exchange through convection determines the vertical oceanic heat flux, which in turn has a direct effect on the ice cover. If determined by plume convection, such flux will occur sporadically and locally for a few days on a horizontal scale of about 500 m (e.g., Marshall and Schott, 1999), and will thus not be detectable with satellite passive-microwave data, not even with the 12 km resolution ASMR.

While providing the unique possibility of verifying an ocean GCMs sea-ice component on the same space and time scales as corresponding satellite-derived products, a basic limitation of the particular approach taken here exists due to the fact that the coarse resolution of the ocean component requires special treatment along the coastline, if such is represented on the fine grid in order to accommodate the high-resolution sea-ice component (Chapter IV). Besides this, there is of course a wealth of other assumptions typically made in a global ocean GCM that may lead to discrepancies from observations. Such include viscosity and diffusivity not being a function of stratification, tidal energy and bathymetry, the lack of a downslope bottom plume parameterization, the lack of an isopycnal mixing parameterization, poor atmospheric forcing fields together with a lack of an atmospheric feedback, and salinity restoring in the upper layer where there is no sea ice.

For improved performances in the high latitudes of climate models, a goal should be to simulate sea ice in a global framework that is coupled to an atmospheric GCM in order to ensure realistic atmospheric feedbacks. From this study it can be concluded that a high-resolution sea-ice component embedded in a coupled atmosphere - ocean GCM should not pose a problem. Since high-resolution satellite-derived ice concentration is routinely available, such setup would allow for a thorough verification of a variable that is highly dependent on the parameterization of subgrid-scale processes that are critical for the long-term ocean circulation, and thus long-term climate change.

Major drawbacks of the current approach include the fact that the atmospheric variables are prescribed. The failure of, e.g., the wintertime air temperature to adjust to a wider polynya will severely overestimate the freezing rate therein. On the other hand, it is not even clear under what assumption on the ambient conditions such a temperature is compiled (e.g., Renfrew et al., 2002; Vihma et al., 2002). The same kind of uncertainty resides with the representation of katabatic winds in NWP analyses. There is also a large uncertainty associated with the freshwater flux as related to the precipitation rates, which modify the snow's insulation effect as well as snow-ice formation (e.g., Powell et al., 2005), and finally its direct impact on the stability of the water column (e.g., Marsland and Wolff, 2001).

Considering the general heterogeneity of a sea-ice cover, one might expect that the strength of the coupling with the atmosphere will change if the ice texture is represented on finer scales. This arises mainly due to the spatially highly inhomogeneous surface variables. E.g., the surface temperature over snow-covered ice can be -30°C in wintertime, while at the same time it is -2°C in a lead. This yields two totally different atmospheric boundary layers, the heat fluxes of the former being such that the surface is essentially decoupled from the atmosphere, while the latter features a highly unstable and strongly coupled situation associated with a major heat loss and thus new-ice formation in the lead. The heat and fresh-water flux forcing of the ocean will thus depend sensitively on the lead fraction (and distribution) and thus ice concentration, which is a prognostic variable of the sea-ice model. Responses to given atmospheric variables or interactions with an atmospheric GCM are thus expected to change with the resolution of a sea-ice model.

A gradual improvement of NWP center (re)analyses, a refinement of the sea-ice grid including the coastline, and an interactive description of the atmospheric forcing fields in a global ocean GCM designed for long-term integrations, will yield ever more reliable estimates on the crucial impact of southern high-latitude processes on intermediate- and deep-ocean climate.

REFERENCES

Aagaard, K., Carmack, E.C., 1994. The Arctic Ocean and climate: a perspective. Geophys. Monogr. 85, 5-20.

Arakawa, A., 1966. Computational design for long-term numerical integration of the equations of fluid motion: two-dimensional incompressible flow. Part I. J. Comput. Phys. 1, 119-143.

Arakawa, A., Lamb, V.R., 1977. Computational design of the basic dynamical processes of the UCLA general circulation model. Methods Comput. Phys. 17, 173-265.

Beckmann, A., Hellmer, H.H., Timmermann, R., 1999. A numerical model of the Weddell Sea: large-scale circulation and water distribution. J. Geophys. Res. 104, 23375-23391.

Brennecke, W., 1921. Die ozeanograpiscen Arbeiten ders Deutschen Expedition 1911-1912. Deut. Seewarte 39 (1), Arch. Hamburg.

Broeke, M.R., Wal, R.S.W., Wild, M., 1997. Representation of Antarctic katabatic winds in a high-resolution GCM and a note on their climate sensitivity. J. Clim. 10, 3111-3130.

Broecker, W.S., 1991. The great ocean conveyor. Oceanography 4, 74-82.

Broecker, W.S., 1997. Thermohaline circulation, the Achilles Heel of our climate system: will man-made CO2 upset the current balance?. Science 278, 1582-1588.

Broecker, W.S., 1999. A possible 20th-century slowdown of Southern Ocean deep water formation. Science 286, 1132-1135.

Canuto, V.M., Howard, A., Hogan, P., Cheng, Y., Dubovikov, M.S., Montenegro, L.M., 2004. Modeling ocean deep convection. Ocean Modelling 7, 75-95, doi:10.1016/S1463-5003(03)00038-6.

Carmack, E.C., Aagaard, K., 1973. On the deep water of the Greenland Sea. Deep Sea Res. 20, 687-715.

Clarke, R.A., Gascard, J.-C., 1983. The formation of Labrador Sea water. Part I: large-scale processes. J. Phys. Oceanogr. 13, 1764-1778.

Comiso, J.C., 1995. SSM/I Sea ice concentrations using the Bootstrap algorithm. NASA Reference Publication 1380.

Comiso, J.C., Cavalieri. D.J., Parkinson, C.L., Gloersen, P. 1997. Passive microwave algorithms for sea ice roncentration - a comparison of two techniques. Rem. Sens. Env. 60, 357-384.

Comiso, J.C., Gordon, A.L., 1998. Interannual variability in summer sea ice minimum, coastal polynyas and bottom water formation in the Weddell Sea,. Antarctic sea ice: physical processes, interactions and variability. AGU, Antarctic Research Series 74, 293-315.

Cunningham, S.A., Alderson, S.G., King, B.A., Brandon, M.A., 2003. Transport and variability of the Antarctic Circumpolar Current in Drake Passage. J. Geophys. Res. 108, C58084, doi: 10.1029/2001JC001147.

Danabasoglu, G., McWilliams, J.C., 1995. Sensitivity of the global ocean circulation to parameterizations of mesoscale tracer transports. J. Clim. 8, 2967-2987.

Delworth, T., Manabe, S., Stouffer, R.J., 1993. Interdecadal variations of the thermohaline circulation in a coupled ocean-atmosphere model. J. Clim. 6, 1993-2011.

Drijfhout, S., Heinze, C., Latif, M., Maier-Reimer, E., 1996. Mean circulation and internal variability in an Ocean Primitive Equation Model. J. Phys. Oceanogr. 26, 559-580.

Duff, P.B., Eby, M., Weaver, A.J., 1999. Effects of salt rejected during formation of sea ice on results of a global ocean-atmosphere-sea ice climate model. Geophys. Res. Let. 26, 739-1742.

Duffy, P.B., Caldeira, K., 1997. Sensitivity of simulated salinity in a three-dimensional ocean model to upper ocean transport of salt from sea-ice formation. Geophys. Res. Lett. 24(11), 1323-1326.

Eisen, O., Kottmeier, C., 2000. On the importance of leads in sea ice to the energy balance and ice formation in the Weddell Sea. J. Geophys. Res. 105 (C6), 14045-14060.

England, M.H., 1993. On the formation of global-scale water masses in ocean general circulation models. J. Phys. Oceanogr. 23, 1523-1552.

Feser, F., Weisse, R., von Storch, H., 2001. Multi-decadal atmospheric modeling for Europe yields multi-purpose data. EOS 82 (28), 305-310.

Foster, T.D., Carmack, E.C., 1976. Frontal zone mixing and Antarctic bottom water formation in the southern Weddell Sea. Deep Sea Res. 23, 301-317.

Fox, A.D., Maskell, S.J., 1996. A nested primitive equation model of the Iceland-Faeroe front. J. Geophys. Res. 101 (C8), 259-278.

Gill, A.E., 1973. Circulation and bottom water production in the Weddell Sea. Deep Sea Res. 20, 111-140.

Gloersen, P., Campbell, W.J., Cavalieri, D.J., Comiso, J.C., Parkinson, C.L., Zwally, H.J., 1992. Arctic and Antarctic sea ice, 1978-1987: satellite passive microwave observations and analysis. Spec. Publ., NASA SP-511, NASA, Washington, D.C.

Goodrick, S.L., McNider, R.T., Schroeder, W.W., 1998. On the interaction of the katabatic-land-sea wind system of Antarctica with the high latitude Southern Ocean. In: Jacobs, S.S., Wiess, R.F. (Eds.), Ocean, ice, and atmosphere: interactions at the Antarctic continental margin. Antarctic Res. Ser. 75, 5-65.

Goosse, H., Fichefet, T., 1999. Importance of ice-ocean interactions for the global ocean circulation: a model study. J. Geophys. Res. 104, 23337-23355.

Goosse, H., Campin, J.-M., Tartinville, B., 2001. The sources of Antarctic bottom water in a global ice-ocean model. Ocean Modelling 3, 95-108.

Goosse, H., Fichefet, T., 2001. Open-ocean convection and polynya formation in a large-scale ice-ocean, model. Tellus 53A, 94-111.

Gordon, A.L., Tchernia, P., 1972. Waters of the continental margin off Adélie Coast, Antarctica, in Antarctic Oceanography II: the Australian-New Zealand Sector. Ant. Res. Ser., vol. 19, edited by Hays, D.E. pp. 59-69. AGU, Washington, D.C.

Gordon, A.L., Huber, B.A., 1990. Southern Ocean winter mixed layer. J. Geophys. Res. 95, 11655-11672.

Gordon, A.L., 1998. Western Weddell Sea thermohaline stratification. In: Jacobs, S.S., Weiss, R.F. (Eds.), Ocean, ice, and atmosphere: interactions at the Antarctic continental margin. Anarctic Res. Ser. 75, 215-240.

Gordon, C., Cooper, C., Senior, C.A., Banks, H., Gregory, J.M., Johns, T.C., Mitchell, J.F.B., Wood, R.A., 2000. The simulation of SST, sea ice extents and ocean heat transports in a version of the Hadley Centre coupled model without flux adjustments. Clim. Dyn. 16, 147-168.

Harms, S., Fahrbach, E., Strass, V.H., 2001. Sea ice transports in the Weddell Sea. J. Geophys. Res. 106, 9057-9073.

Heil, P., Hibler III, W.D., 2002. Modeling the high-frequency component of Arctic sea ice drift and deformation. J. Phys. Oceanogr. 32, 3039-3057.

Hibler, W.D., 1979. A dynamic thermodynamic sea ice model. J. Phys. Oceanogr. 9, 815-846.

Hirst, A.C., Cai, W., 1994. Sensitivity of a world ocean GCM to changes in subsurface mixing parameterization. J. Phys. Oceanogr. 24, 1256-1279.

Hu, D., 1997. Global-scale water masses, meridional circulation, and heat transport simulated with a global isopycnal ocean model. J. Phys. Oceanogr. 27, 96-120.

Jacob, D., Podzun, R., 1997. Sensitivity studies with the regional climate model REMO. Meteorol. Atmos. Phys. 63, 119-129.

Jacobs, S.S., Amos, A.F., Bruchhausen, P.M., 1970. Ross Sea oceanography and Antarctic bottom water formation. Deep Sea Res. 17, 935-962.

Jacobs, S.S., Fairbanks, R.G., Horibe, Y., 1985. Origin and evolution of water masses near the Antarctic continental margin: evidence from $H_2^{18}O/H_2^{16}O$ ratio in Sea water. In: Jacobs S.S., Weiss, R.F. (Eds.) Oceanology of the Antarctic Continental Shelf. Antarctic Res. Ser. 43, 59-85.

Jiang, L., Garwood, R.W., 1995. A numerical study of three-dimensional dense water bottom plumes on a Southern Ocean continental slope. J. Geophys. Res. 100, 18471-18488.

Killworth, P.D., 1983. Deep convection in the world ocean. Rev. Geophys. 21 (1), 1-26.

Kim, S.-J., Crowley, T.J., Stössel, A., 1998. Local orbital forcing of Antarctic climate change during the last interglacial. Science 280, 728-730.

Kim, S.-J., Stössel, A., 2001. Impact of subgrid-scale convection of global thermohaline properties and circulation. J. Phys. Oceanogr. 31,656-674.

Koentopp, M., Eisen, O., Kottmeier, C., Padman, L., Lemke, P., 2005. Influence of tides on sea ice in the Weddell Sea: investigations with a high-resolution dynamic-thermodynamic sea ice model. J. Geophys. Res., 110, C02014, doi:10.1029/2004JC002405.

Large, W.G., Danabasoglu, G., Doney, S.C., 1997. Sensitivity to surface forcing and boundary layer missing in a global ocean model: annual-mean climatology. J. Phys. Oceanogr. 27, 2418-2447.

Levitus, S., 1982. Climatological atlas of the World Ocean. NOAA Prof. Paper no. 13, 173pp.

Maier-Reimer, E., 1993. The driving force of brine rejection on the deepwater formation in the Hamburg LSG OGCM. NATO-ASI series, It12, pp. 211-216.

Maier-Reimer, E., 1997. Design of a closed-boundary regional model of the Arctic Ocean. Bull. Amer. Meteor. Soc., Workshop on polar processes in global climate, 13-15 November 1996, pp. 72-73.

Manabe, S., Stouffer, R.J., 1996. Low-frequency variability of surface air temperature in a 1000-year integration of a coupled atmospere-ocean-land surface model. J. Clim. 9, 376-393.

Markus, T., Cavalieri, D.J., 2000. An enhancement of the NASA Team sea ice algorithm. IEEE Trans. Geosc. and Remote Sens. 38 (3), 1387-1398.

Markus, T., Kottmeier, C., Fahrbach, E., 1998. Ice formation in coastal polynyas in the Weddell Sea and their impact on oceanic salinity. Antarctic sea ice: physical processes, interactions and variability. AGU, Antarctic Research Series 74, 273-292.

Marshall, J., Schott, F., 1999. Open-ocean convection: observations, theor, and models. Rev. Geophys. 37.1-64.

Marsland, S., Wolff, J.-O., 2001. On the sensitivity of Southern Ocean sea ice to the surface fresh-water flux: A model study. J. Geophys. Res. 106 (C2), 2723-2741.

Marsland, S.J., Haak, H., Jungclaus, J.H., Latif, M., Roeske, F., 2003. The Max-Planck-Institute global ocean / sea ice model with orthogonal curvilinear coordinates. Ocean Modelling 5 (2), 91-127.

Martinson, D.G., 1990. Evolution of the Southern Ocean winter mixed layer and sea ice: open-ocean deep water formation and ventilation. J. Geophys. Res. 95, 11641-11654.

Mikolajewicz, U., Jngclaus, J., Haak, H., 2001. Simulating the ocean response to atmospheric variability. WMO/TD No. 1064, Report No. 31, pp. 9.18-9.19.

Mosby, H., 1934. The waters of the Atlantic Antarctic Ocean. Sec. Res. Norw. Antarct. Exped. 1927-1928, 1 (11), 131pp.

Ogura, T., Abe-Ouchi, A., Hasumi, H., 2004. Effects of sea ice dynamics on the Antarctic sea ice distribution in a coupled ocean atmosphere model. J. Geophys. Res. 109, C04025, doi: 10.1029/2003JC002022.

Orsi, A.H., Johnson, G.C., Bullister, J.L., 1999. Circulation, mixing, and production of Antarctic bottom water. Progr. Oceanogr. 43, 55-109.

Orsi, A.H., Jacobs, S.S., Gordon, A.L., Vsbeck, M., 2001. Cooling and ventilating the abyssal ocean. Geophys. Res. Lett. 28 (15), 2923-2926.

Orsi, A.H., Smethie Jr., W.M., Bullister, J.L., 2002. On the total input of Antarctic waters to the deep ocean: a preliminary estimate from chlorofluorocabon measurements. J. Geophys. Res. 107, 10.1029/2001JC000976.

Orsi, A.H., Whitworth III, T., 2004. Hydrographic Atlas of the World Ocean Circulation Experiment (WOCE). Volume 1: Southern Ocean (Eds.) Sparrow, M., Chapman, P., Gould, J., Inernational WOCE Porect Office, Southampton, U.K., ISBN 0-904175-49-9.

Owens, W.B., Lemke, P., 1990. Sensitivity studies with a sea ice - mixed layer - pycnocline model in the Weddell Sea. J. Geophys. Res. 95, 9527-9538.

Padman, L., Kottmeier, C., 2000. High frequency ice motion and divergence in the Weddell Sea. J. Geophys. Res. 105, 3379-3400.

Paluszkiewicz, T., Romea, R.D., 1997. A one-dimensional plume model for the parameterization of oceanic deep convection. Dyn. Ocean Atmos. 26, 95-130.

Parish, T.R., Bromwich, D.H., 1991. Continental-scale simulation of the Antarctic katabatic wind regime. J. Clim. 4, 135-146.

Parkinson, C.L., Washington, W.M., 1979. A large-scale numerical model of sea ice. J. Geophys. Res. 84, 311-337.

Powell, D.C., Markus, T., Stössel, A., 2005. The effects of snow depth forcing on Southern Ocean sea ice simulations. J. Geophys. Res., 110(C6), C06001.

Reid, J.L., 1996. On the circulation of the South Atlantic Ocean. In: the South Atlantic: present and past circulation. (Eds.) Wefer, G., Berger, W. H., Siedler, G., Webb, D. J., 13-44. Springer-Verlag, Berlin Heidelberg.

Reid, J.L., Lynn, R.L., 1971. On the influence of the Norwegian-Greenland and Weddell Seas upon the bottom waters of the Indian and Pacific Oceans. Deep Sea Res. 18, 1063-1088.

Renfrew, I.A., King, J.C., Markus, T., 2002. Coastal polynyas in the southern Weddell Sea: variability of the surface energy budget. J. Geophys. Res. 107 (C6), 3063, doi:10.1029/2000JC000720.

Seidov, D., Barron, E., Haupt, B.J., 2001. Meltwater and the global ocean conveyor: northern versus southern connections. Global and Planetary Change 30, 257-270.

Semtner, A.J., Jr., 1976. A model for the thermodynamic growth of sea ice in numerical investigations of climate. J. Phys. Oceanogr. 6, 379-389.

Spall, M.A., Holland, W.R., 1991. A nested primitive equation model for oceanic applications. J. Phys. Oceanogr. 21, 205-220.

Stommel, H., 1962. On the smallness of sinking regions in the ocean. Proc. Nat. Acad. Sci. U.S.A. 48, 766-772.

Stössel, A., Owens, W.B., 1992. The Hamburg sea-ice model. (Eds), Modellbetratungsgrupe, Tech. Rep. No. 3, 61 pp., Edutsches Klimarechenzentrum.

Stössel, A., Kim, S.-J., Drijfhout, S., 1998. The impact of southern ocean sea ice in a global ocean model. J. Phys. Oceanog. 28 (10), 1999-2018.

Stössel, A., Kim, S.-J., 2001. Decadal deep-water variability in the subtropical Atlantic and convection in the Weddell Sea. J. Geophys. Res. 106 (C10), 22425-22440.

Stössel, A., Yang, K., Kim, S.-J., 2002. On the role of sea ice and convection in a global ocean model. J. Phys. Oceanogr. 32, 1194-1208.

Stössel, A., Markus, T., 2004. Using satellite-derived ice concentration to represent Antarctic coastal polynyas in ocean climate models. J. Geophys. Res. 109, C02014, doi: 10.1029/2003JC001779.

Stössel, A., Kim, J.-T., 2006. Enhancing the resolution of sea ice in a global ocean GCM. Ocean Modelling 11 (1-2), 28-48.

Stössel, A., Stössel, M.M., Kim, J.-T., 2007. High-resolution sea ice in long-term global ocean GCM integrations. Ocean Modelling 16 (3-4), 206-223.

Strass, V.H., Fahrbach, E., 1998. Temporal and regional variation of sea ice draft and coverage in the Weddell Sea obtained from upward looking sonars. Antarctic sea ice: physical processes, interactions and variability. AGU, Antarctic Research Series 74, 123-139.

Timmermann, R., Hellmer, H.H., Beckmann, A., 2002. Simulations of ice-ocean dynamics in the Weddell Sea 2. Interannual variability 1985-1993. J. Geophys. Res., 107. 10.1029/2000JC000742.

Timmermann, R., Beckmann, A. 2004. Parameterization of vertical mixing in the Weddell Sea. Ocean Modelling 6 (1), 83-100.

Timmermann, R., Goosse, H., Madec, G., Fichefet, T., Ethe, C., Duliere, V., 2005. On the representation of high latitude processes in the ORCA-LIM global coupled sea-ice - ocean model. Ocean Modelling 8, 175-201.

Toggweiler, J.R., Samuels, B., 1995. Effects of sea ice on the salinity of Antarctic Bottom Waters. J. Phys. Oceanogr. 25, 1980-1997.

Vihma, T., Uotila, B., Cheng, B., Launiainen, J., 2002. Surface heat budget over the Weddell Sea: buoy results and model comparisons. J. Geophys. Res. 107 (C2), 2000JC000372.

Washington, W.M., Meehl, G.A., 1996. High-latitude climate change in global coupled ocean-atmosphere-sea ice model with increased atmospheric CO_2. J.Geophys. Res. 101, 12795-12801.

Withworth, III, T., Peterson, R.G., 1985. Volume transport of the Antarctic circumpolar current from bottom pressure measurements. J. Phys. Oceanogr. 15, 810-816.

Whitworth, T., Orsi, A.H., Kim, S.-J., Nowlin, W.D., Locarnini, R.A., 1998. Water masses and mixing near the Antarctic slope front. In: Jacobs, S.S., Weiss, R.F. (Eds.), Ocean, ice and atmosphere: interactions at the Antarctic continental margin. Antarctic Res. Ser. 75, 1-27.

Wolff, J.-O., Maier-Reimer, E., Legutke, S., 1997. The Hamburg Ocean Primitive Equation model HOPE. Technical Report No. 13, Hamburg/Germany: Deutsches Kimarechenzentrum.

VITA

Name: Joong Tae Kim

Address: Department of Oceanography,

Texas A&M University, 3146 TAMU, c/o Achim Stössel

College Station, TX 77843, USA

E-mail Address: julian_kim@yahoo.com

Education: B.S., Physics, Hanyang University at Seoul, 1985

M.S., Physics (Acoustics), Ohio University, 1989